Check for updates

Wiley
Advances in Civil Engineering
Volume 2024, Article ID 8534390, 21 pages
https://doi.org/10.1155/adce/8534390

WILEY

Research Article

Strength Prediction of Geopolymer Concrete With Wide-Ranged Binders and Properties Using Artificial Neural Network

Md Merajul Islam[1], **Md Al-Mamun Provath**[2], **G. M. Sadiqul Islam**[1] and **Md Tariqul Islam**[1]

[1]*Department of Civil Engineering, Chittagong University of Engineering and Technology (CUET), Chattogram 4349, Bangladesh*
[2]*Department of Computer Science and Engineering, Chittagong University of Engineering and Technology (CUET), Chattogram 4349, Bangladesh*

Correspondence should be addressed to G. M. Sadiqul Islam; gmsislam@cuet.ac.bd

Received 13 June 2024; Accepted 2 December 2024

Academic Editor: Suvash Chandra Paul

Copyright © 2024 Md Merajul Islam et al. This is an open access article distributed under the Creative Commons Attribution License, which permits unrestricted use, distribution, and reproduction in any medium, provided the original work is properly cited.

Geopolymer concrete (GPC) is an efficient alternative to traditional construction materials, utilizing amorphous or semicrystalline waste–based binders. It enhances durability than Portland cement, remaining environment friendly and cost-effective, while promoting waste reuse. Despite extensive use and research, predicting concrete strength based on the mixed chemical composition of constituents remains challenging due to consideration of limited variables, small dataset sizes, and traditional models struggling with nonlinearity. The primary objective is to develop an artificial neural network (ANN) model to enhance the accuracy of compressive strength (C-S) predictions of GPC, which is crucial for the sustainable use of waste-based binders in construction. For this, the study incorporates a comprehensive dataset of 1018 experimental data points of binary and ternary GPC from 43 research sources addressing these issues. Thirteen input parameters, including three major geopolymer binder's oxide compositions (viz, SiO_2, CaO, and Al_2O_3), are considered to generalize the model across various binder types. With all these, an ANN model was developed to handle the inherent nonlinearity of input parameters, validated through fivefold cross-validation. The relationship between individual parameters and C-S is analyzed. Additionally, regression models (viz., linear regression (LR), Lasso regression, Ridge regression, and XGBoost regressor) were developed to thoroughly assess the performance of the ANN model in comparison to the conventional regression model. The ANN model, superior to other regression techniques, excels in recognizing nonlinear correlations between features and an objective variable, a challenge for traditional regression models. Various metrics assess model performance (e.g., mean absolute error (MAE), root mean square error (RMSE), mean square error (MSE), *R*-squared (R^2)), revealing the ANN model's superiority over regression models. The ANN model's proficiency in nonlinear correlations contributes to its effectiveness, yielding low MAE ($=2.58$), RMSE ($=4.13$), and MSE ($=17.86$) values, and high ($R^2=0.93$) value, signifying minimal deviation between predicted and actual C-S values. By focusing on the oxide composition of binders, the model is more generalized, making it applicable across different binder types and not limited to specific materials. Also, the parametric analysis confirmed the ANN's ability to capture the effects of input parameters, offering a comprehensive prediction tool. This study highlights the potential of employing the ANN model for predicting material behavior, offering a resource-efficient approach, and showcasing the viability of mixed GPC for sustainable industrial waste utilization. Future research directions include exploring the model's application under varying environmental conditions and expanding the dataset to enhance its diversity and representativeness.

Keywords: artificial neural network (ANN); cross-validation; geopolymer concrete (GPC); regression techniques; supplementary cementitious materials (SCM)

1. Introduction

With the current rate, the increasing demand for cement is expected to double by 2050 [1]. However, the production of constituent materials and reactions during the Portland cement hydration process considerably affects the greenhouse effect [2, 3]. Depending on the technology used for manufacture, production of one tone of cement produces 0.7–1 tone of carbon dioxide (CO_2) [4–6], which also contributes 5%–9% of the world's CO_2 emissions [7–9]. Thus, it is essential to explore substitute materials for cement that have the same binding capabilities to reduce environmental impact [10–13].

Geopolymer concrete (GPC) became one of the most important alternatives for reducing CO_2 emissions from the concrete construction sector. Aluminosilicate sources, including fly ash (FA), metakaolin (MK), and ground granulated blast furnace slag (GGBS), are combined with an alkaline liquid activator, such as sodium hydroxide (NH) or sodium silicate (NS), during the geopolymerization process [14]. From recent studies, GPC could have improved performance, durability properties, and lower carbon emissions than traditional Portland cement concrete. For instance, Mehta et al. [15] improved the compressive strength (C-S) of FA-GGBS–based GPC up to 52% and reduced the chlorine penetration up to 78% through heat curing process by optimizing mix proportion using Taguchi method. Guo et al. [16] investigated fiber reinforced MK–based geopolymer composite and found that the optimum mix of MK–based geopolymer composite with hybrid fiber could have a strength gain up to 160% by inhibiting development of microcracks. According to Albitar et al. [17], GPC produced with FA and ground lead smelter slag (GLSS) is more resistant to acid and chemical attacking than OPC concrete. GPC with bioadditives has significant durability against sulfate and chemical attack [18]. Adak, Sarkar, and Mandal [19] investigated how GPC interacts with nanomaterials. Ahmed, Mohammed, and Mohammed [20] reported that adding nanosilica increased mechanical strength by 21% compared to the control GPC mixture by improving microstructure and inhibiting fracture development. In comparison to cement, the application of supplementary cementitious materials (SCMs) in the production of GPC can lower CO_2 emissions up to 5–6 times [21] as the majority of these SCMs are waste or byproducts created during the production of other goods or a process. According to the studies, GPC may minimize power consumption by up to 15%, while maintaining indoor temperature [22]. Utilizing these SCMs in concrete reduces environmental hazards, while producing durable concrete [11, 23].

Due to its potential benefits to the environment and economy, GPC is now an active area of research to obtain the intended mechanical characteristics of GPC by investigating a mixture composition and a suitable constituent selection in a laboratory setting. Several parameters influence the mechanical properties of GPC, such as NH and NS concentration, alkaline liquid-to-binder ratio (l/b), binder quantity, composition, the buffering ability of the alkaline liquids [24], and temperature [2]. It is observed that GPC is greatly dependent on the kind of binder used due to the variation in oxide composition. For instance, the study showed that C-S increases with CaO content when FA is partially replaced by CaO-rich precursors like GGBS [25]. Increasing SiO_2 content leads to microstructures with low porosity, improving the strength of GPC [26]. C-S of GPC also depends on the NH concentration, with a study by Prasanphan et al. [27] showing that 10 M NH yields the highest strength for calcined kaolin processing waste-based GPC. According to Mohammed, Ahmed, and Mosavi [28], the curing process considerably affects the strength of AAMs. Higher initial curing temperatures and durations (generally 24 h) led to better C-S [29]. Aliabdo, Abd Elmoaty, and Salem [30] reported 0.4 as an optimal alkaline liquid-to-binder (l/b) ratio for GPC, while Phoongernkham et al. [31] noticed a decrease in C-S in the increase of l/b ratio from 0.4 to 0.9. It can be observed from the study of Nikoloutsopoulos et al. [32] that C-S of GPC is related to various parameters such as binder content, fine and coarse aggregate content, NH concentration, NS to NH ratio, water-to-binder ratio, and curing temperature. However, all these laboratory tests were often expensive, time-consuming, and not always feasible to examine all the mix proportions with various ingredients, thus, creating a lack of relationship between different input parameters and the desired mechanical characteristics of GPC.

In the recent two decades, experts have heavily favored data-driven techniques, particularly artificial neural network (ANN) [33, 34], to predict desirable outcomes, in particular about the mechanical strength of GPC [35–40]. ANN is a computational model that simulates the functioning of the human brain and is useful for resolving complex engineering problems [41]. Predictive modeling utilizing ANN generally does not explicitly express the particular model equation [42]; instead, it analyses the relationship between variables and automatically processes the training data. Because of this, it is crucial to gather considerable experimental data for modeling [43]. For instance, Topçu and Saridemir [44] used ANN and fuzzy logic (FL) models to predict the 7, 28, and 90-day C-Ss of FA–based GPC. Likewise, Prasad, Eskandari, and Reddy [45] created an ANN model to predict the 28-day C-S of a high-volume FA–based concrete. de Cos Juez et al. [46] investigated using an AAN approach to predict the C-S of ceramic waste concrete. Likewise, Nazari and Torgal [47] and Yadollahi, Benli, and Demirboğa [48] used AANs to predict the mechanical characteristics of GPC and found that ANN can efficiently predict the mechanical properties of GPC as well. Nagajothi and Elavenil [49] developed a predictive ANN model for predicting the mechanical strength of FA and GGBS–based GPC with M-Sand as fine aggregate from his experimental data points. Additionally, several researchers have looked into how ANNs can be used to predict the properties of geopolymers [48, 50–52]. Like, Ahmed, Mohammed, and Mohammed [53] proposed different models like ANN, linear regression (LR), non-LR (NLR), and M5P-tree to forecast the C-S of GPC containing nanosilica, whereas ANN seems to be the most prominent. According to several studies, the ANN model can carry out the prediction of different outcomes with more reasonable accuracy [45, 54, 55]. Data-driven techniques previously employed to predict desirable outcomes for concrete manufacturing with SCMs are summarized in Table 1.

Most of these studies were not able to gather a significant amount of data, and all of them are restricted to some extent to

7074, 2024, 1, Downloaded from https://onlinelibrary.wiley.com/doi/10.1155/adce/8534390 by Bangladesh Hinari NPL, Wiley Online Library on [25/01/2025]. See the Terms and Conditions (https://onlinelibrary.wiley.com/terms-and-conditions) on Wiley Online Library for rules of use; OA articles are governed by the applicable Creative Commons License

Table 1: Data-driven techniques have previously been used to predict the desirable outcomes of GPC.

Refs.	Year	Data points	Materials used	Algorithm used	Prediction properties
[44]	2007	180	High-lime and low-lime FAs	ANN	C-S
[45]	2007	300	FA	ANN	C-S
[46]	2012	—	Ceramic waste powder	ANN	C-S
[47]	2012	399	Tungsten mine wastes, MK	ANN	C-S
[48]	2016	45	Pumice powder	ANN	C-S
[56]	2021	60	Ceramic waste powder	ANN	C-S
[57]	2009	179	MK	ANN	C-S
[58]	2013	32	Nanosilica	ANN	C-S
[50]	2009	40	MK	ANN	C-S
[51]	2014	50	Alumina silicate	ANN	C-S
[59]	2021	144	FA	SVM	C-S
[60]	2021	642	FA	GEP, ANN, DT	Chloride concentration
[61]	2020	—	FA	SVM	C-S
[62]	2020	351	Steel slag	GEP	C-S
[62]	2020	54	Natural zeolite	GEP	C-S
[63]	2019	205	FA, steel slag, RHA	ANN	C-S
[64]	2019	131	FA, steel slag	RF	C-S
[65]	2017	114	FA	ANN	C-S
[66]	2017	69	FA	ANN	C-S
[67]	2021	270	FA	GEP, DT	C-S
[43]	2012	144	FA, RHA	ANN	C-S
[68]	2008	45	Steel slag	ANN	C-S
[42]	2015	283	FA, steel slag	ANN, MVR	C-S
[69]	2009	48	SF	ANN, FL	C-S
[70]	2008	195	MK, SF	ANN	C-S
[71]	2019	36	FA	ANN	Setting time
[71]	2019	273	FA	ANN	C-S
[71]	2019	72	FA	ANN	Peak heat
[53]	2022	207	Nanosilica	ANN, LR, NLR, M5P-tree	C-S
[49]	2019	20	FA, steel slag	ANN	C-S
[72]	2019	210	FA	ANFIS, ANN	C-S
[This study]	2023	1018	Geopolymer precursors	ANN	C-S

Abbreviations: ANN, artificial neural network; C-S, compressive strength; DT, decision tree; FA, fly ash; FL, fuzzy logic; GEP, gene expression programming; GPC, geopolymer concrete; LR, linear regression; MK, metakaolin; MVR, multivariable regression; NLR, nonlinear regression; RF, random forest; RHA, rice husk ash; SF, silica fume; SVM, support vector machine.

the binder type (Table 1). Also, these studies cannot comprehend all the parameters affecting the C-S of GPC. Thus, a more reliable approach is necessary for better understanding and predicting the useful combination of GPC. In this regard, computational modeling [73], the parametric multivariable regression (MVR) model, and artificial intelligence (AI) [74] can be employed to overcome these shortcomings.

Thus, this study aims to explore the use of ANN for predicting the C-S of GPC using the 1018 data collected from previous literature and apply a wide range of input parameters that may affect the C-S of GPC and evaluate its accuracy compared to traditional regression models. This study includes three major oxide components as input parameters to make the model more generalize to be useful for all kinds of SCMs. Additional efforts were made to understand better the factors that influence the C-S of GPC. The ANN model showed high accuracy with less variance than traditional regression models when opting for the available data. ANN methods provide a more precise prediction of material strength qualities, while requiring less sample casting and testing time. In addition, these models can effectively work on the same nature of data irrespective of the type of materials or variables considered for the input. The findings of these studies are anticipated to promote the utilization of GPC, which could lead to a more efficient combination of cementitious materials and sustainable construction practices by reducing waste and improving the quality of the final product.

2. Methodology

The present research was intended to develop a reliable ANN algorithm for predicting the C-S of GPC. Experimental data from the literature was obtained randomly to achieve unbiased representation. Published articles on similar materials were chosen, focusing on predicting the C-S of GPC. A wide range of input parameters covering all the influencing factors for

7074, 2024, 1, Downloaded from https://onlinelibrary.wiley.com/doi/10.1155/adce/8534390 by Bangladesh Hinari NPL, Wiley Online Library on [25/01/2025]. See the Terms and Conditions (https://onlinelibrary.wiley.com/terms-and-conditions) on Wiley Online Library for rules of use; OA articles are governed by the applicable Creative Commons License

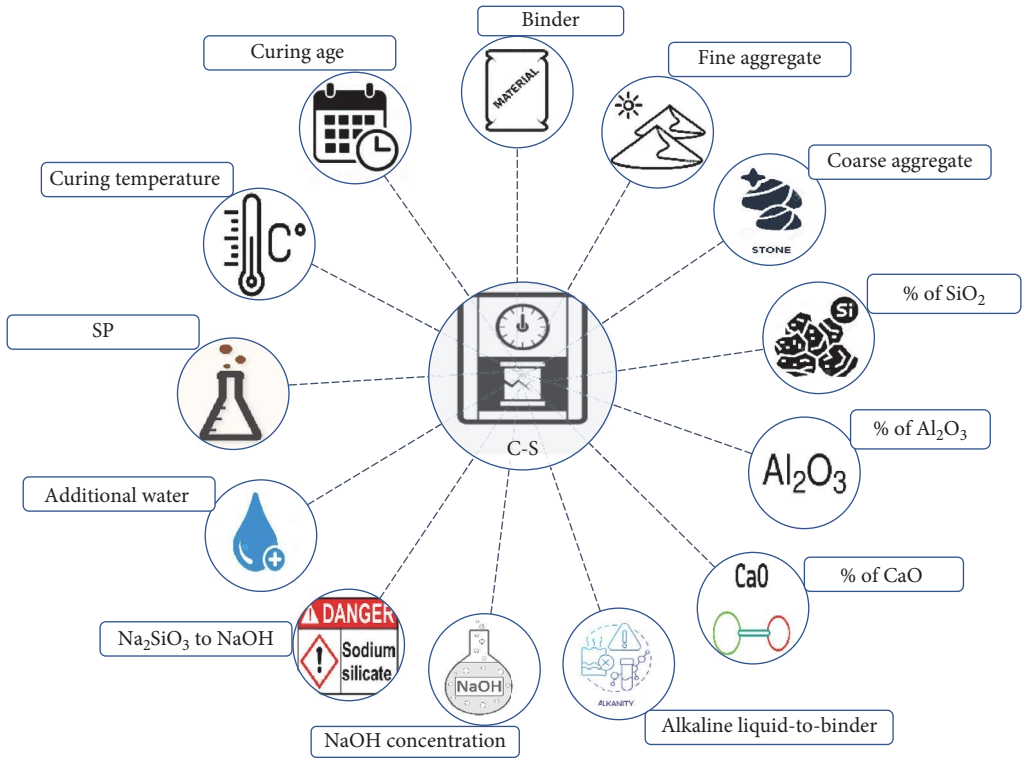

FIGURE 1: Factors affecting compressive strength (C-S) of geopolymer concrete (GPC). SP, superplasticizer.

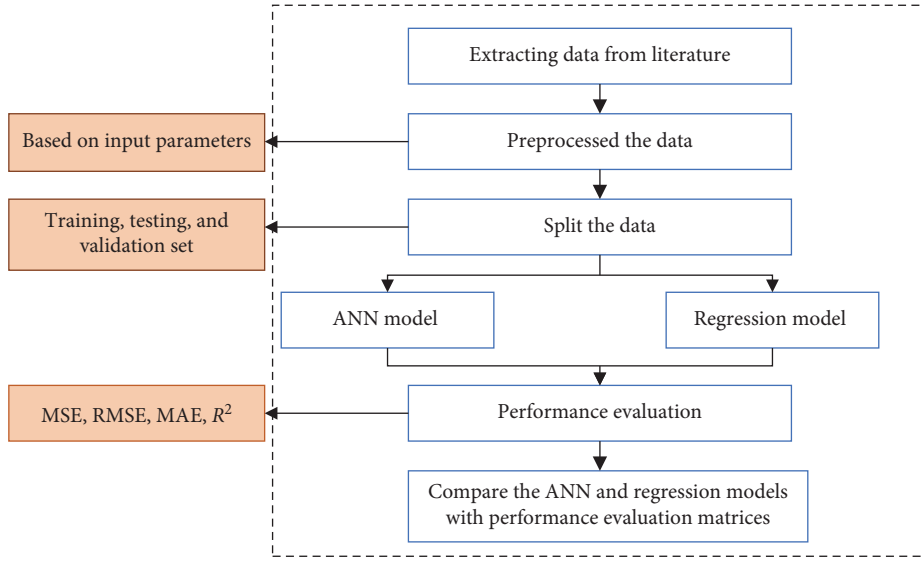

FIGURE 2: Overview of the methodology of this study. ANN, artificial neural network; MAE, mean absolute error; MSE, mean square error; R^2, *R*-squared; RMSE, root mean square error.

GPC was considered when developing a model. Four regression models were developed alongside the ANN model for a comprehensive comparison. The research seeks to create a generalized predictive model for GPC, excluding the binder type and emphasizing the three major chemical components, namely, % of SiO_2, Al_2O_3, and CaO. Figure 1 illustrates various factors that influence C-S of GPC. The methodology flowchart is illustrated in Figure 2.

2.1. Data Collection. This study utilized a dataset of 1018 experimentally collected C-S values from various compositions of GPC under ambient curing conditions. The dataset was compiled from 43 publications, focusing initially on binary and ternary geopolymer mixtures. The chemical composition of binders was analyzed for three major oxides: SiO_2, CaO, and Al_2O_3. Model predictions exclusively targeted the C-S of concrete, with values standardized to a 150 mm cube size using a

7074, 2024, 1, Downloaded from https://onlinelibrary.wiley.com/doi/10.1155/adce/8534390 by Bangladesh Hinari NPL, Wiley Online Library on [25/01/2025]. See the Terms and Conditions (https://onlinelibrary.wiley.com/terms-and-conditions) on Wiley Online Library for rules of use; OA articles are governed by the applicable Creative Commons License

Table 2: Inputs and output parameters for the artificial neural network (ANN) model.

Input parameters	Units
Binders amount	kg/m^3
Fine aggregate-to-binder	—
Coarse aggregate-to-binder	—
SiO_2	% of binder
Al_2O_3	% of binder
CaO	% of binder
Alkaline liquid-to-binder (l/b ratio)	—
Sodium hydroxide (NH) molarity	Molar (M)
Sodium silicate (NS) to NH ratio	—
Additional water to binder	% of binder
Superplasticizer (SP)-to-binder	% of binder
Curing temperature	°C
Curing ages	Days
Output parameters	**Units**
Compressive strength (C-S)	MPa

conversion factor given by Yi, Yang, and Choi [75]. The current study used an incredibly diverse data set, comprising geopolymer binder composition to curing conditions to mix proportion; at the same time, it acknowledges that overrepresentation exists regarding particular binder types, such as FA and GGBS. It may bring biases that could impact model performance when applied to other binder types, for example, slag or silica fume (SF). Biases of this type can be minimized, making this model more applicable universally by increasing data to include many different types of geopolymer binders in future studies. Input and output parameters were structured for ANN development, with data then segregated into training, validation, and testing sets. This facilitated the assessment of machine learning approaches in predicting the C-S for each concrete type. Table 2 gives details of the parameters considered. In contrast, Table 3 presents the characteristics of the input and output variables of a construction material, and the relative frequency distribution of input variables is shown in Figure 3.

2.2. Data Preprocessing. Data preprocessing, a pivotal phase in research, encompasses tasks such as data cleansing, scaling, and normalization, with the overarching goal of augmenting dataset quality and utility. Identifying and removing numerous extraneous columns unaligned with research objectives constituted a critical step. Subsequently, the chosen feature columns underwent Min–Max normalization to ensure uniform scale and range, expediting convergence in training deep learning models and averting feature dominance. It effectively expedited convergence and reduced the possibility of gradient explosion during training. Equation (1) gives the normalization formula applied for this purpose. Figure 4 depicts the correlation heatmap for various input and output parameters. Most variable pairs exhibit weak correlations.

The feature "Binder amount" shows a strong negative correlation (−0.72) with another feature "fine aggregate to binder ratio." This suggests that the related feature decreases significantly as the amount of binder increases, indicating an inverse relationship. "% of CaO" shows moderate correlations (0.40), implying that these factors also play a meaningful role in strength development.

$$X_{\text{scaled}} = \frac{x - X_{\min}}{X_{\max} - X_{\max}}. \tag{1}$$

Here, X_{scaled} is the normalised data, $X_{\min}$ is the minimum value of the vector, and $X_{\max}$ is the maximum value of the vector.

Standardization, transforming the data with a mean of 0 and a standard deviation 1 was applied. Normalization and standardization minimize the bias from features with more extensive numerical ranges, promoting balanced learning across all input parameters and improving model stability.

2.3. Data Partitioning Using Stratified Fivefold Cross-Validation. Each model underwent validation through the rigorous stratified fivefold cross-validation methodology. Test cases comprised 20% of the dataset, leaving 80% for training and validation. An 80/20 split was maintained within the training dataset, allocating 80% for actual training and 20% for validation. Figure 5 visually portrays the intricate data partitioning scheme adopted. This strategic approach facilitated a robust model evaluation by employing diverse data subsets during training and testing.

2.4. Regression Technique. Regression models can be categorized as either linear or nonlinear, although the latter can be transformed into linear models by applying various methods. Developing reliable predictions using NLR models requires a priori knowledge of the model's degree or adopting appropriate assumptions. The equation for multiple LR is presented in Equation (2).

$$Y = b_0 + b_1X_1 + \ldots\ldots\ldots\ldots + b_nX_n + \varepsilon. \tag{2}$$

In model equation,
Y = dependent variable,
X_i = independent variable,
b_i = calculated coefficient parametrs,
ε = error term.

In this work, four regression models were developed, namely, LR, Lasso regression, Ridge regression, and extreme gradient boosting regression (XGBRegressor), to compare the performance of the ANN model. These models represent linear and nonlinear modeling approaches. First, the inclusions of linear, Ridge, and Lasso regressions create a baseline understanding of how the model handles linear correlations. XGBoost was chosen because it can handle nonlinear relationships, given that it serves as an excellent benchmark to compare the ANN model against.

2.5. ANN Model Architecture. The architectural design of an ANN model encompasses an input layer, one or more hidden

7074, 2024, 1, Downloaded from https://onlinelibrary.wiley.com/doi/10.1155/adce/8534390 by Bangladesh Hinari NPL, Wiley Online Library on [25/01/2025]. See the Terms and Conditions (https://onlinelibrary.wiley.com/terms-and-conditions) on Wiley Online Library for rules of use; OA articles are governed by the applicable Creative Commons License

Table 3: The characteristics of input data.

Variables	Minimum	Maximum	Mean	Standard deviation
Input variables				
Fine aggregate-to-binder	1	2.75	1.73	0.31
Coarse aggregate-to-binder	1.65	3.64	2.87	0.36
Binder (kg)	318	508	396.08	29.75
SiO_2 (%)	27.56	92.21	48.12	8.88
CaO (%)	0.51	43.39	16.59	10.49
Al_2O_3 (%)	0.38	32.43	21.79	5.74
l/b ratio	0.28	0.79	0.42	0.06
Sodium hydroxide (NH) molarity	0.5	19	9.81	3.45
Sodium silicate (NS) to NH	0.33	4.26	1.89	0.7
Additional water-to-binder (%)	0	51.5	5.58	8.56
Superplasticizer (SP) to binder (%)	0	7	1.78	2.21
Curing temperature (°C)	20	35	24.02	3.22
Age (days)	1	90	19.99	18.84
Output variable				
Compressive strength (C-S; MPa)	0	83	30.22	16.35

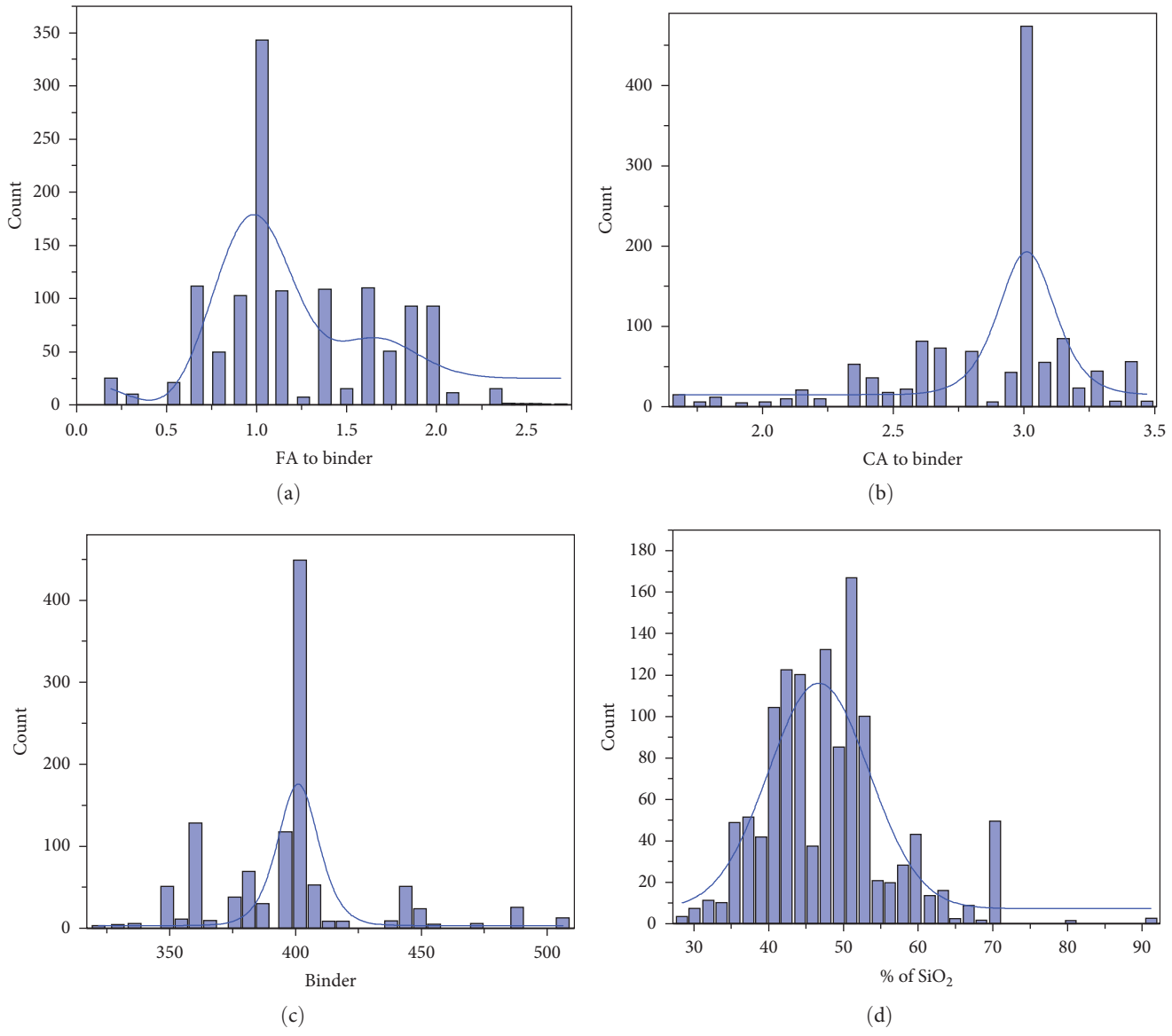

Figure 3: Continued.

7074, 2024, 1, Downloaded from https://onlinelibrary.wiley.com/doi/10.1155/adce/8534390 by Bangladesh Hinari NPL, Wiley Online Library on [25/01/2025]. See the Terms and Conditions (https://onlinelibrary.wiley.com/terms-and-conditions) on Wiley Online Library for rules of use; OA articles are governed by the applicable Creative Commons License

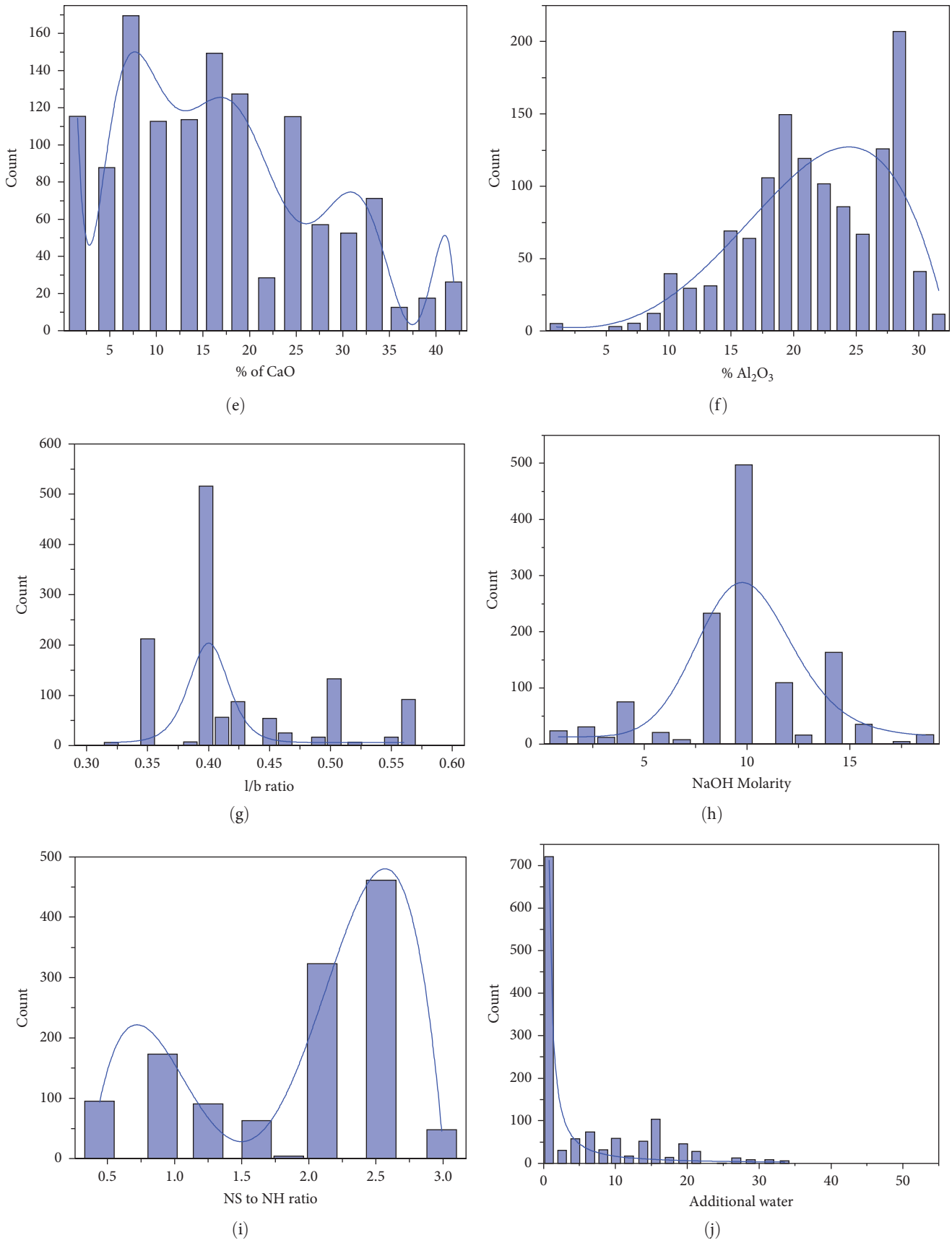

Figure 3: Continued.

7074, 2024, 1, Downloaded from https://onlinelibrary.wiley.com/doi/10.1155/adce/8534390 by Bangladesh Hinari NPL, Wiley Online Library on [25/01/2025]. See the Terms and Conditions (https://onlinelibrary.wiley.com/terms-and-conditions) on Wiley Online Library for rules of use; OA articles are governed by the applicable Creative Commons License

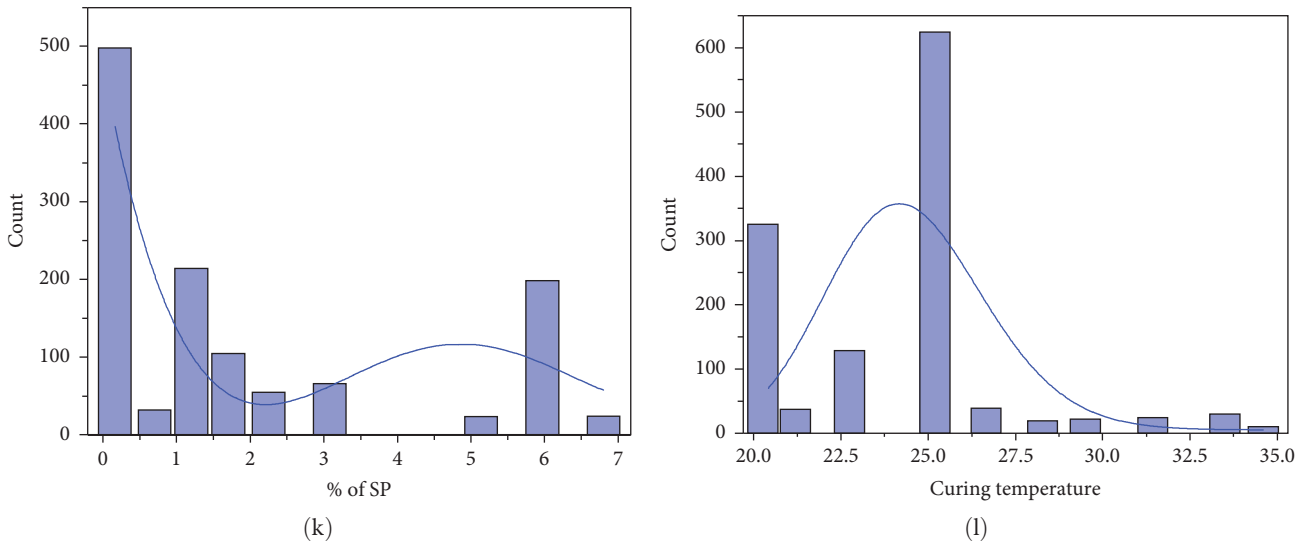

FIGURE 3: Relative frequency distribution of input variables (a–l). FA, fly ash; NH, sodium hydroxide; NS, sodium silicate; SP, superplasticizer.

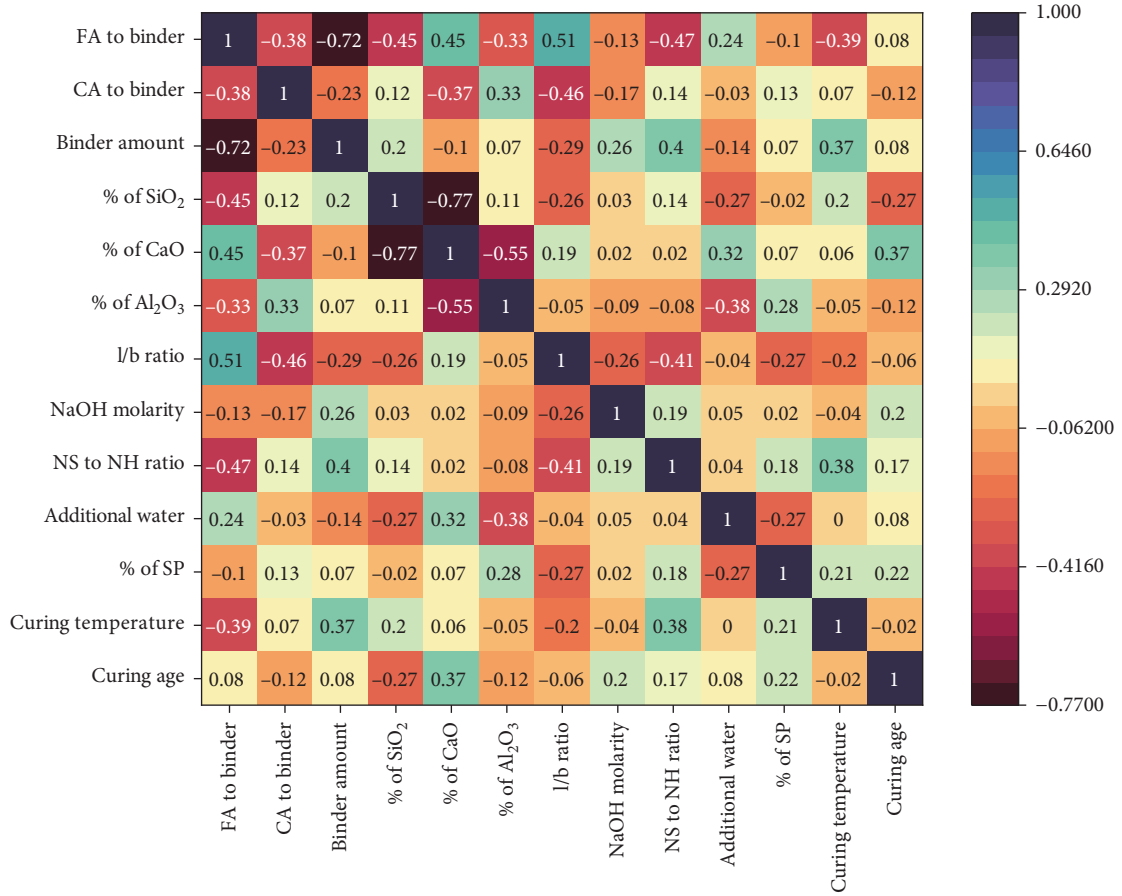

FIGURE 4: Correlation heatmap of input parameters. FA, fly ash; NH, sodium hydroxide; NS, sodium silicate; SP, superplasticizer.

layers, and an output layer [76]. The input layer ingests the raw data, while the hidden layers execute the computational engine, performing complex mathematical operations to generate the final output in the output layer. The representation of n inputs applied to a neuron as $X = X_1, X_2 \ldots\ldots\ldots X_n$, where the weight for input X_j is represented as W_j and the bias as b, yields the output of the neuron as specified by Equation (3), with the neurons being connected through connection links featuring weights multiplied by the transmitted signal in the network.

7074, 2024, 1, Downloaded from https://onlinelibrary.wiley.com/doi/10.1155/adce/8534390 by Bangladesh Hinari NPL, Wiley Online Library on [25/01/2025]. See the Terms and Conditions (https://onlinelibrary.wiley.com/terms-and-conditions) on Wiley Online Library for rules of use; OA articles are governed by the applicable Creative Commons License

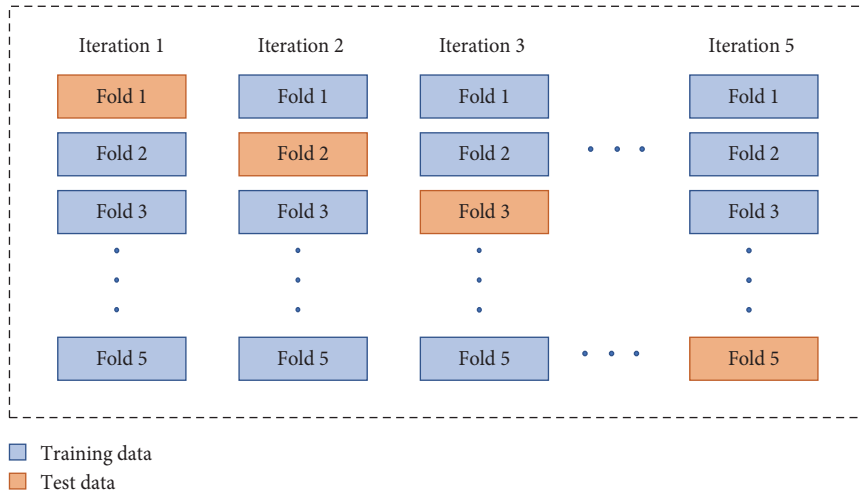

FIGURE 5: Data partitioning using stratified fivefold cross-validation.

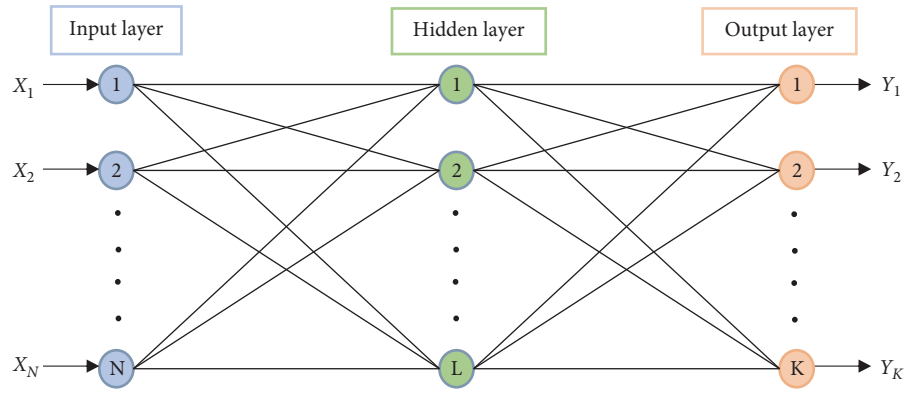

FIGURE 6: Artificial neural network (ANN) model architecture. Adopted from de Cos Juez et al. [46].

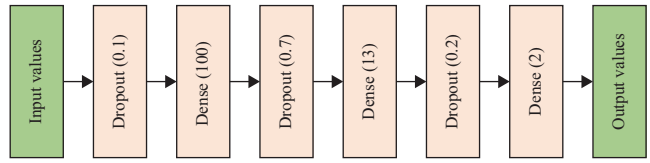

FIGURE 7: Artificial neural network (ANN) base model configuration.

$$Y = f\sum_{j=0}^{n}\left(X_j W_j - b\right). \tag{3}$$

The activation function employed in the context of ANNs is the logistic function given in Equation (4).

$$f(x) = \frac{e^{x} - e^{-x}}{e^{x} + e^{-x}}. \tag{4}$$

Throughout the training process, the weight adjustment rate is initially highest, gradually decreasing until it converges to zero, indicating a stable output despite variations in input. This relationship is described by Equation (5).

$$W_t = W_{t-1} - L_t.\Delta C_t. \tag{5}$$

Conducting the ANN model training process results in formulating a mathematical expression representing the model for C-S, denoted as Equation (6).

$$\text{C-S} = f(\text{input parameters}). \tag{6}$$

The architecture of the ANN model is given in Figure 6, and the configuration of the base model is shown in Figure 7.

7074, 2024, 1, Downloaded from https://onlinelibrary.wiley.com/doi/10.1155/adce/8534390 by Bangladesh Hinari NPL, Wiley Online Library on [25/01/2025]. See the Terms and Conditions (https://onlinelibrary.wiley.com/terms-and-conditions) on Wiley Online Library for rules of use; OA articles are governed by the applicable Creative Commons License

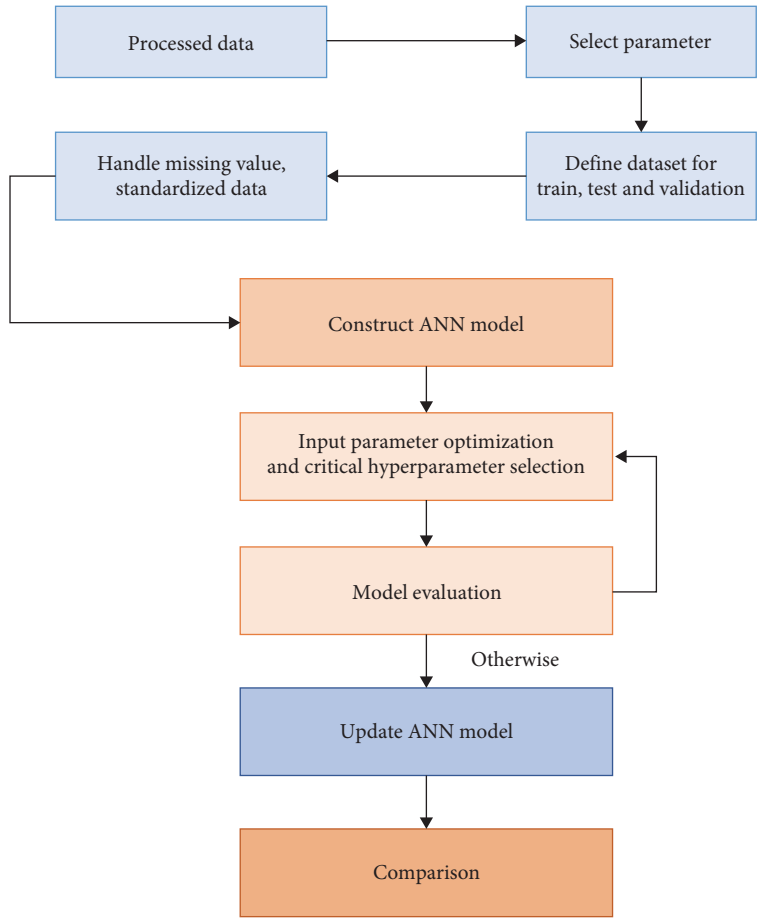

FIGURE 8: Steps for evaluating model performance. ANN, artificial neural network.

Several important techniques were applied to improve the model's performance and prevent overfitting. First, a dropout layer was used, which randomly deactivated some neurons during training. This allows the model to rely more on specific features. Additionally, the application of L2 regularization kept the model simple by reducing large weights. Early stopping was also used to monitor the model's performance and stop training when it no longer improves. A k-fold cross-validation was used. These methods ensure that the model remains reliable, while handling unseen data.

2.6. Model Performance Evaluation. The evaluation of model performance in machine learning is a crucial step that requires a structured methodology to assess the accuracy of a model's predictions on new and unseen data, which can be influenced by various factors depicted in Figure 8. These include input features, data preprocessing techniques, model architecture, and hyperparameters, necessitating several steps for comprehensive performance evaluation.

2.7. Performance Evaluation Metrics. Evaluating the performance of the developed ANN in accurately predicting the targeted output of the test data requires determining multiple types of errors, including mean absolute error (MAE), mean square error (MSE), root mean square error (RMSE), R-squared (R^2), and a20 index, as per Equations (7)–(11). Lower errors, as indicated by metrics such as MAE, MSE, and RMSE, signify reduced deviation between predicted and actual values, suggesting a more precise prediction capability of the model. Conversely, a higher R^2 value reflects a stronger correlation between predicted and observed values, implying a better overall fit of the model to the test data and enhancing confidence in its predictive performance.

$$\text{MAE} = \frac{1}{n}\sum_{i=1}^{n}|x_i - y_i|. \tag{7}$$

$$\text{MSE} = \frac{1}{n}\sum_{i=1}^{n}|x_i - y_i|^2. \tag{8}$$

$$\text{RMSE} = \sqrt{\text{MSE}}. \tag{9}$$

$$R^2 = 1 - \frac{\sum_{i=1}^{n}(y_i - \widehat{y}_i)^2}{\sum_{i=1}^{n}(y_i - \overline{y})^2}. \tag{10}$$

$$a20 - \text{index} = \frac{m20}{M}. \tag{11}$$

7074, 2024, 1, Downloaded from https://onlinelibrary.wiley.com/doi/10.1155/adce/8534390 by Bangladesh Hinari NPL, Wiley Online Library on [25/01/2025]. See the Terms and Conditions (https://onlinelibrary.wiley.com/terms-and-conditions) on Wiley Online Library for rules of use; OA articles are governed by the applicable Creative Commons License

Table 4: Different artificial neural network (ANN) model configuration.

Model	Number of neurons in dense layer	Activation function in dense layer	Batch size	Optimizer
Model 1	17	tanh	4	Adam
Model 2	15		4	Adagrad
Model 3	14		8	Adam
Model 4	13		4	RMSProp
Model 5	20		8	Adagrad
Model 6	19		4	RMSProp

3. Results and Discussion

3.1. Dataset Diversity and Representativeness. The dataset used for this study comprises 70% FA and GGBS as the primary binder materials. The remaining 30% is composed equally of SF, rice husk ash (RHA), and MK, creating a more balanced representation of SCMs. This proportion highlights a particular bias toward FA and GGBS due to their higher presence in the data. However, the oxide composition within the binder materials is well-distributed, with SiO_2 ranging between 30%–50%, CaO between 2%–35%, and Al_2O_3 between 10%–30%. This well-balanced range of oxide percentages helps somewhat mitigate the bias, ensuring the model captures the variability in binder chemistry rather than focusing too narrowly on specific materials. Additionally, more than 807 data points (around 80%) correspond to a C-S range between 0 and 50 MPa, with the remaining 20% in the 50–80 MPa range. While this ensures low to moderate-strength range coverage, the model is underrepresented in high-strength GPC. It is also important to note that the dataset primarily includes ambient curing conditions without any data related to steam curing, even though steam curing is known to enhance the performance of GPC. This limits the generalizability of the model to curing conditions that do not take advantage of thermal treatments, which may be critical in some applications of GPC.

3.2. Implementation Environment. The outcomes produced by this model undergo a meticulous examination, juxtaposed against state-of-the-art methodologies, thereby, substantiating the efficacy inherent in the approach. Implementing the proposed method in Python 3.9 unfolds within the Linux operating ecosystem. It is pertinent to highlight that the training and testing procedures transpire within the confines of a robust computing environment. This high-performance computational setup ensured the efficient processing of complex neural network applications. It also provided reliable performance evaluation, validating the accuracy and robustness of the model (Table 4).

3.3. Model Performance Analysis Using Loss Curve. Figure 9 gives a visual representation of the temporal evolution of MAE in training and validation contexts over 50 epochs, thereby, affording profound insights into the intricate dynamics governing the model's cognitive assimilation and identifying potential refinements within its didactic progression. The graphical illustration shows the model's bias towards convergence as it endeavors to minimize MAE systematically with the incremental amplification of training epochs. The overarching objective is

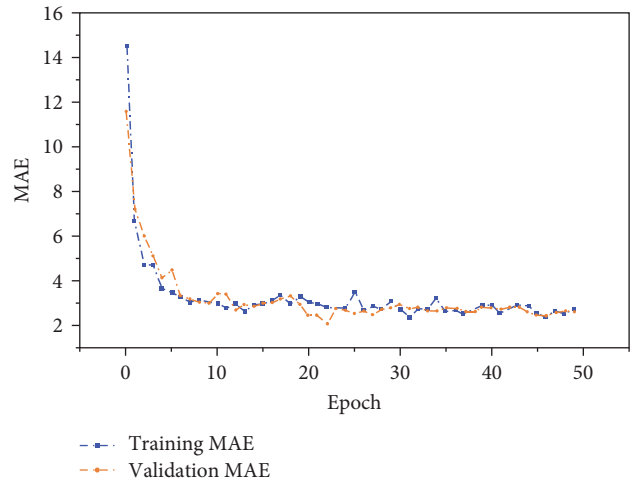

Figure 9: Training and validation (mean absolute error (MAE)) vs. Epoch.

Table 5: Impact of normalization.

	Impact of normalization			
	MAE	MSE	RMSE	R^2
Without normalization	5.69	19.58	6.94	0.88
With normalization	**2.58**	**17.86**	**4.13**	**0.93**

Abbreviations: MAE, mean absolute error; MSE, mean square error; R^2, *R*-squared; RMSE, root mean square error.

the attenuation of both training and validation MAE to their utmost minima, thereby, establishing a cognitive state wherein the model not only adeptly generalizes to previously unseen data but also mitigates the peril of overfitting—a condition wherein the model excessively tailors itself to the idiosyncrasies of the training dataset, resulting in suboptimal performance when confronted with novel instances.

3.4. Impact of Normalization. Table 5 gives an unequivocal demonstration of performance enhancement when employing data normalization compared to utilizing unnormalized data. This underscores the pivotal role of applying this particular data preprocessing technique in amplifying the efficiency and reliability of diverse analytical processes, thereby, accentuating the critical significance of addressing data disparities to engender more robust and accurate outcomes.

3.5. Hyperparameter Tuning. Hyperparameter tuning, an essential aspect of optimizing machine learning, entails finely

7074, 2024, 1, Downloaded from https://onlinelibrary.wiley.com/doi/10.1155/adce/8534390 by Bangladesh Hinari NPL, Wiley Online Library on [25/01/2025]. See the Terms and Conditions (https://onlinelibrary.wiley.com/terms-and-conditions) on Wiley Online Library for rules of use; OA articles are governed by the applicable Creative Commons License

Table 6: The values of tuned hyper-parameters used in the artificial neural network (ANN) model.

Hyper-parameters	Value
Number of neurons in dense layer 1	100
Number of neurons in dense layer 2	19
Number of neurons in dense layer 3	190
Percentage of dropout in layer 1	0.1
Percentage of dropout in layer 2	0.7
Percentage of dropout in layer 3	0.2
Learning rate	0.001
Batch size	4
Optimizer	Adam

adjusting parameters to find an equilibrium between model complexity and generalization. Table 6 provides the values of the tuned hyperparameters used to develop the ANN model. Table 4 summarizes the configurations of ANN models utilized in this research study to predict an outcome variable. The fine-tuned hyperparameters for the ANN model present a comprehensive setup, including a first dense layer with 100 neurons, a second layer with 19 neurons, and a third layer with 190 neurons. Incorporating dropout layers with dropout rates of 0.1, 0.7, and 0.2, respectively, alongside a learning rate of 0.001 and a batch size of 4, along with the Adam optimizer, reflects a meticulous optimization strategy aimed at achieving accuracy and generalization in predictive tasks. The diverse configurations of the ANN models, ranging from varying numbers of neurons in dense layers to distinct activation functions and optimization strategies, underscore the nuanced approach to model design aimed at effectively addressing specific data complexities and achieving optimal performance across different tasks and datasets (Table 4). This searches for the best ANN architecture and its hyperparameters so that more robust model performance can be obtained. The network architecture consists of various hidden layers with ReLU as the activation function to grasp the nonlinear dependencies of data effectively. Dropout layers are used with rates 0.1, 0.7, and 0.2 to avoid overfitting by deactivating neurons at random during training. This was also a reason to use the Adam optimizer, because it uses an adaptive learning rate heuristic, it would make the model converge faster on one hand but would prevent it from getting stuck into a local minimum.

Figure 10 presents the prediction performance metrics for three optimization algorithms: RMSProp, Adam, and Adagrad. The comparative analysis shows that Adam outperforms both RMSProp and Adagrad in between these three metrics, with the lowest metrics value. Figure 11 presents the performance metrics of the ANN model for two different batch sizes. The results demonstrate that a batch size of 4 performs better than a batch size of 8 in terms of error value.

The prediction performances of different ANN models for the testing set are shown in Table 7. Model 6 achieved the lowest values for all three metrics, indicating that Model 6 is the most accurate predictor of the outcome variable. Also, suggesting that RMSProp may be the most effective optimizer for this specific prediction task. The subsequent utilization of

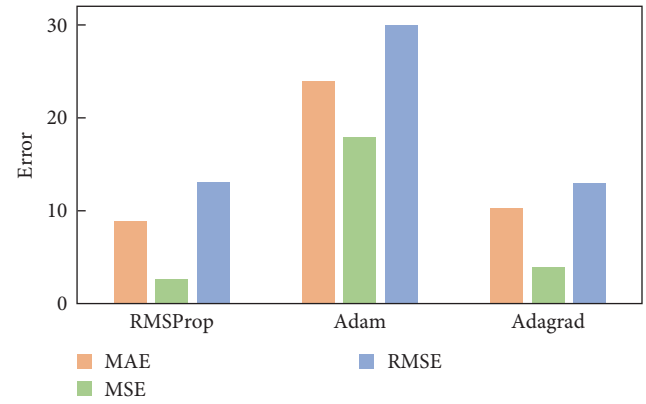

Figure 10: Different optimizer performance comparison. MAE, mean absolute error; MSE, mean square error; RMSE, root mean square error.

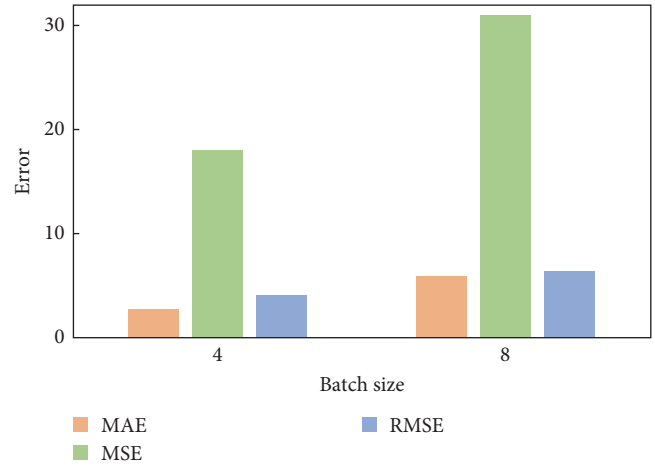

Figure 11: Batch size performance comparison. MAE, mean absolute error; MSE, mean square error; RMSE, root mean square error.

Table 7: The prediction performances of ANN models for the testing set.

ANN Models	Optimizer	Performance evaluation metrics		
		MAE	MSE	RMSE
Model 1	Adam	8.26	94.82	9.73
Model 2	Adagrad	13.16	19.01	13.04
Model 3	Adam	8.36	32.55	10.84
Model 4	RMSProp	8.26	32.87	9.95
Model 5	Adagrad	9.25	23.86	13.78
Model 6	RMSProp	2.58	17.86	4.13

Abbreviations: ANN, artificial neural network; MAE, mean absolute error; MSE, mean square error; RMSE, root mean square error.

ANN testing results has been meticulously represented in Figure 12. The performance of the proposed Model 6 was evaluated using several statistical indices, including the a20 index [77], which measures the proportion of predictions within a ±20% deviation from the actual values. The a20 index

7074, 2024, 1, Downloaded from https://onlinelibrary.wiley.com/doi/10.1155/adce/8534390 by Bangladesh Hinari NPL, Wiley Online Library on [25/01/2025]. See the Terms and Conditions (https://onlinelibrary.wiley.com/terms-and-conditions) on Wiley Online Library for rules of use; OA articles are governed by the applicable Creative Commons License

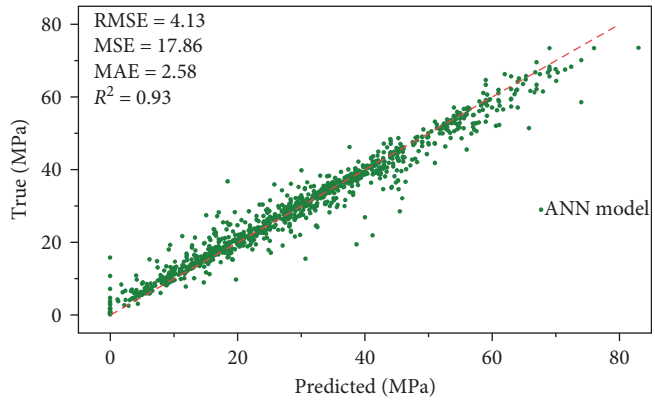

Figure 12: Model prediction with artificial neural network (ANN) model 6. MAE, mean absolute error; MSE, mean square error; RMSE, root mean square error.

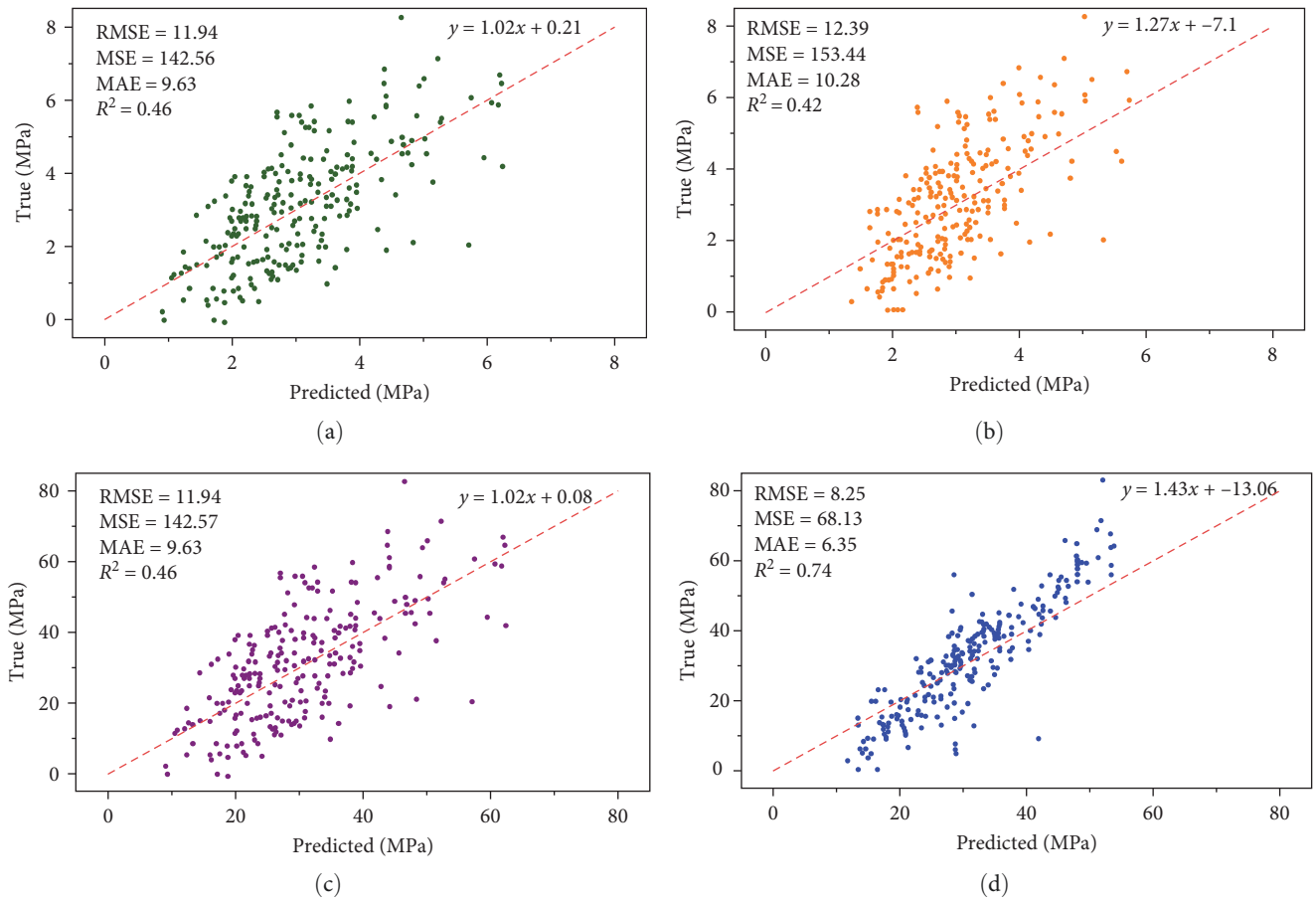

Figure 13: Model prediction with regression output; (a) LR, (b) Lasso regression, (c) Ridge regression, (d) XGBoost regressor. LR, linear regression; MAE, mean absolute error; MSE, mean square error; RMSE, root mean square error.

for the proposed model was found to be 0.91, indicating that 91% of the predictions fell within the acceptable ±20% range of the actual values, demonstrating high predictive accuracy.

3.6. Proposed Model Performance Comparison With Regression Methods. The predictive capabilities of various regression models for the testing set are presented in Figure 13. Essential details about the regression models' performance are revealed from their evaluation. The ANN model exhibits the best accuracy with an RMSE of 4.13, trailed by the XGBoost regressor at 8.25. The RMSE measures the average magnitude of errors between predicted and observed values. The Lasso regression performs marginally worse with an RMSE of 12.39, while the LR and Ridge regression have the same

7074, 2024, 1, Downloaded from https://onlinelibrary.wiley.com/doi/10.1155/adce/8534390 by Bangladesh Hinari NPL, Wiley Online Library on [25/01/2025]. See the Terms and Conditions (https://onlinelibrary.wiley.com/terms-and-conditions) on Wiley Online Library for rules of use; OA articles are governed by the applicable Creative Commons License

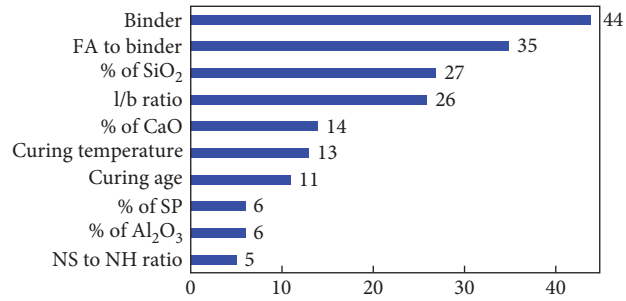

FIGURE 14: Features importance comparison. FA, fly ash; NH, sodium hydroxide; NS, sodium silicate; SP, superplasticizer.

RMSE of 11.94. A similar pattern was noted in terms of MSE, which is the average of the squared disparities between anticipated and actual values. The ANN model surpasses the other models with an MSE of 17.86. The XGBoost regressor comes in second with an MSE of 68.13, followed by the LR and Ridge regression with MSEs of 142.56 each. The Lasso regression has a somewhat higher MSE (153.44).

The MAE indicates the average of the absolute disparities between predicted and actual values. The ANN model has the highest accuracy, with an MAE of 2.58. The XGBoost regressor is next, with an MAE of 6.35, followed by LR and Ridge regression with an MAE of 9.63. The Lasso regression has a significantly higher MAE, 10.28.

The R^2 values reflect the proportion of the variance in the dependent variable that is foreseeable from the independent variables. The ANN model shines with an R^2 of 0.93, accounting for 93% of the variance. The XGBoost regressor follows with an R^2 of 0.74, while the LR and Ridge regression have an R^2 of 0.46. The Lasso regression has the lowest explained variance, with an R^2 value of 0.42.

The salient features that make ANN outperform the conventional regression models are essentially due to the inherent abilities of ANN to capture complex nonlinear correlations among many variables, which the conventional LR models handle inadequately. In general, the regression models such as linear, Ridge, and Lasso are indeed suitable for modeling when the linearity is part of the process; however, in understanding the nonlinearities of the parameters such as oxide composition, binder ratio, and curing temperatures, they have serious drawbacks. On the other hand, ANN correctly classifies such subtlety due to its multilayer network, which can learn higher levels of abstract features through backpropagation and nonlinear activation functions.

Upon comparing the performance of these models, the evaluation metrics indicate that the ANN model is the most accurate and reliable among the regression models for this dataset, followed by the XGBoost regressor. It becomes evident that the ANN models consistently outperform traditional regression models across all evaluation metrics. This observation implies that, in this particular problem's context, ANN models are a superior choice for forecasting the outcome variable when juxtaposed with conventional regression models.

Figure 14 depicts the feature importance analysis for the concrete strength prediction model using XGBoost. "Binder amount" exhibits the highest importance score (44.0), indicating that the amount of binder used significantly influences the C-S of GPC. This is expected, as the binder is a primary component in the concrete mix, contributing to its overall structural integrity. With a score of 35.0, the feature "fine aggregate to binder ratio" suggests that the type and amount of fine aggregate binder used can substantially affect strength outcomes. The features "% of SiO_2" (27.0) and "alkaline liquid-to-binder" (26.0) highlight the importance of the chemical composition and activator solutions in the geopolymer mixture. SiO_2 content plays a pivotal role in the pozzolanic reactions, enhancing the strength and durability of the concrete. "% of CaO" (14.0) and "curing temp" (13.0) suggest that the chemical properties of the binder and the curing conditions are vital for achieving optimal C-S. Proper curing conditions can enhance the bonding and strength development in GPC. Features such as "age" (11.0), "% of SP" (6.0), "% of Al_2O_3" (6.0), and "Na_2SiO_3_by_NaOH" (5.0) have lower importance scores, indicating that while they may contribute to C-S, their influence is less pronounced compared to the top features.

It reveals that the binder amount exhibits the most prominent influence with an impressive *F*-score of 44.0, closely trailed by the fine aggregate-to-binder ratio boasting an *F*-score of 35.0, underscoring the pivotal roles these elements play in dictating the robustness of concrete compositions. Furthermore, factors such as % of SiO_2, l/b ratio, and % of CaO also demonstrate considerable significance, with *F*-scores of 27.0, 26.0, and 14.0, respectively, highlighting the intricate interplay of various constituents in shaping the overall strength characteristics of concrete materials.

TABLE 8: Performance comparison with Asteris and Kolovos [63].

	MAE	MSE	RMSE	R^2
Asteris and Kolovos [63]	—	—	—	0.982
This study	0.035	1.052	1.021	0.993

Abbreviations: MAE, mean absolute error; MSE, mean square error; R^2, *R*-squared; RMSE, root mean square error.

3.7. Proposed Model Comparison With Existing Literature. The performance of the proposed ANN model was rigorously assessed using two challenging datasets. The first dataset, sourced from Asteris and Kolovos [63], demonstrated the model's effectiveness, with a higher R^2 value compared to existing models, as shown in Table 8 and Figure 15. Similarly, the second dataset from Yeh [78] corroborated these findings, as evidenced by the comparative output analysis in Table 9 and the visual representation in Figure 16, further underscoring the robustness and superior predictive capability of our ANN model.

3.8. Parametric Analysis of C-S With Input Parameters Using ANN Model. Parametric analysis of C-S with the input variables was performed to observe the trend of C-S with the change in input variables. Changes in C-S were determined through the ANN model by varying a single input parameter from its minimum to maximum range and keeping the other parameters constant. The graphical representation of the parametric analysis is given in Figure 17.

7074, 2024, 1, Downloaded from https://onlinelibrary.wiley.com/doi/10.1155/adce/8534390 by Bangladesh Hinari NPL, Wiley Online Library on [25/01/2025]. See the Terms and Conditions (https://onlinelibrary.wiley.com/terms-and-conditions) on Wiley Online Library for rules of use; OA articles are governed by the applicable Creative Commons License

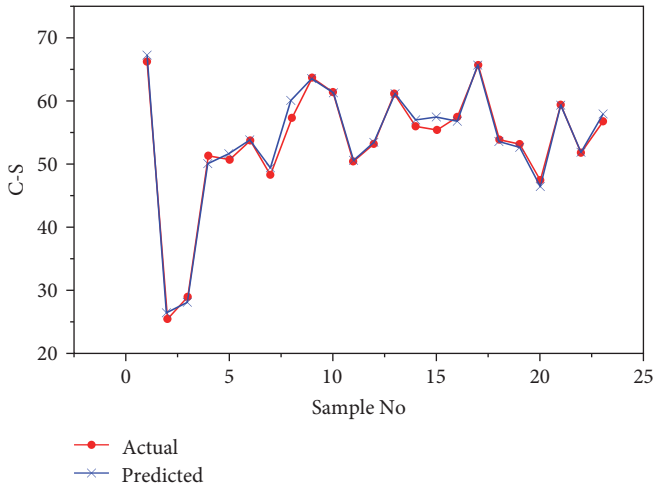

Figure 15: Actual vs. predicted values of compressive strength (C-S) [63].

Table 9: Performance comparison with Yeh [78].

	MAE	MSE	RMSE	R^2
Yeh [78]	—	—	—	0.814
This study	1.435	4.052	2.012	0.915

Abbreviations: MAE, mean absolute error; MSE, mean square error; R^2, *R*-squared; RMSE, root mean square error.

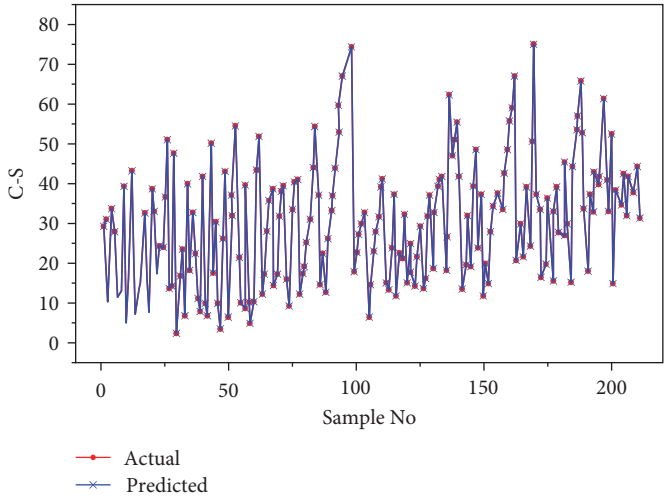

Figure 16: Actual vs. predicted values of compressive strength (C-S) [78].

As shown in Figure 17a, C-S abruptly decreases beyond the 420 kg/m^3 binder. Figure 17b,c represents that increasing fine aggregate content increases the C-S, whereas a concrete aggregate-to-binder ratio of more than three could decrease the C-S. From Figure 17d–f, the amount of CaO was found to be the main influential factor that affect the C-S significantly. Das et al. [79] showed in their study that in ternary GPC, an increase of RHA, which contains more than 95% SiO_2, would decrease C-S. Figure 17g indicates l/b ratio 0.35–0.4 gives the optimum C-S. In their experimental study, Jithendra and Elavenii [76] reported a similar trend for the l/b ratio, whereas Nath and Sarker [80] showed a different trend for the l/b ratio. Figure 17h,i shows that NH concentration from 8 to 12 M and NS to NH ratio 2–2.5 performs better for obtaining C-S. Ling et al. [71] found a similar trend for NH concentration and NS to NH ratio, whereas he showed that increasing NH concentration would increase C-S even after 20 M. Reddy and Murugan [81] showed that C-S increases with NS to NH ratio then decreases with further increase of NS to NH. Niş [82] reported the effect of NS to NH varies with the NH concentration. As shown in Figure 17j,k, additional water up to 8% could lower the C-S at a significantly slower rate, whereas increasing SP beyond 3% could potentially increase the C-S. Figure 17j–l shows that the variation of curing temperature from 20 to 30°C has minimal impact on the strength of GPC. Figure 17m indicates that C-S increases with age but gains most of its strength during the first 28 days of the curing period, which is also supported by the previous study [71, 80, 83]. Khan et al. [84] also explained the parametric analysis of different influencing factors.

3.9. Implications of Results. The results of this study reveal that the ANN model significantly outperforms traditional regression models in predicting the C-S of GPC. This has several important implications for the academic community and practical engineering applications [85]. One of the key reasons is its ability to capture complex, nonlinear interactions between input and output variables. Traditional regression models often struggle with these nonlinear relationships. The ANN model demonstrates the potential of machine learning approaches for material property predictions. This insight could influence future material studies to increasingly adopt AI–based models, especially when dealing with complex formulations. The ANN model's predictive accuracy offers engineers a practical tool for designing optimal GPC mixes. The model can help engineers optimize the mix design without requiring extensive experimental trials by accurately predicting the C-S based on varying input parameters. This can lead to more cost-effective and time-efficient processes in developing sustainable construction materials.

This research highlights the importance of data-driven decision-making in civil engineering. Machine learning models such as ANN can yield more reliable predictions, especially with large datasets. The ANN model's generalizability suggests that it can be applied across different datasets and types of GPC binders, making it a valuable tool for C-S prediction and potentially for other performance metrics such as tensile strength or durability under various environmental conditions. This model's success in predicting C-S using oxide compositions as input parameters can be transferred to other construction materials with similar compositional complexity. This approach can potentially accelerate the adoption of AI in material science, where machine learning models are used to predict and optimize material properties, further reducing reliance on traditional empirical methods.

Future research could explore developing hybrid models that combine ANN with other machine learning techniques, such as genetic algorithms (GAs) or support vector machines (SVMs), to further improve the accuracy and robustness of GPC strength predictions. These hybrid approaches could

7074, 2024, 1, Downloaded from https://onlinelibrary.wiley.com/doi/10.1155/adce/8534390 by Bangladesh Hinari NPL, Wiley Online Library on [25/01/2025]. See the Terms and Conditions (https://onlinelibrary.wiley.com/terms-and-conditions) on Wiley Online Library for rules of use; OA articles are governed by the applicable Creative Commons License

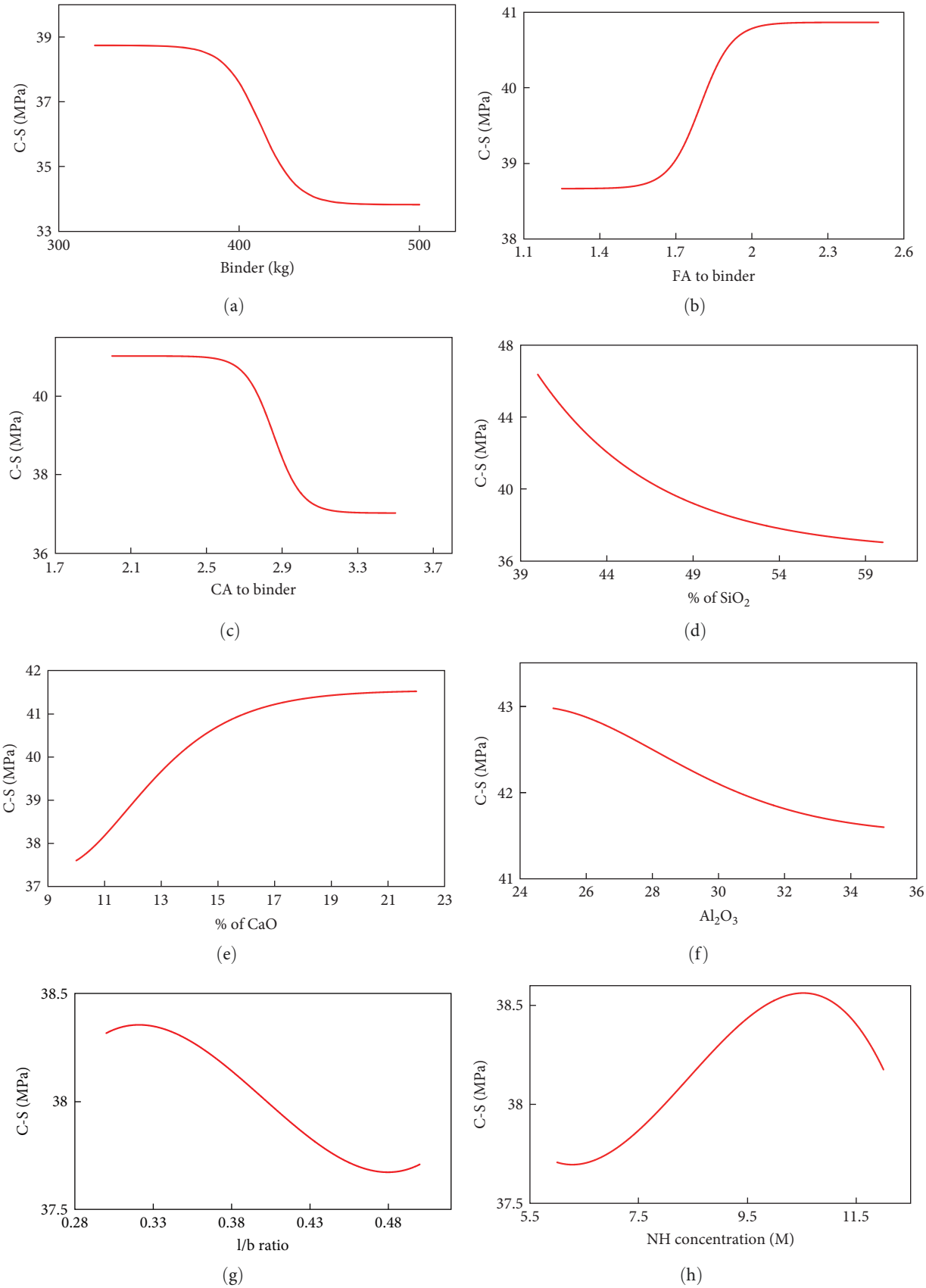

Figure 17: Continued.

7074, 2024, 1, Downloaded from https://onlinelibrary.wiley.com/doi/10.1155/adce/8534390 by Bangladesh Hinari NPL, Wiley Online Library on [25/01/2025]. See the Terms and Conditions (https://onlinelibrary.wiley.com/terms-and-conditions) on Wiley Online Library for rules of use; OA articles are governed by the applicable Creative Commons License

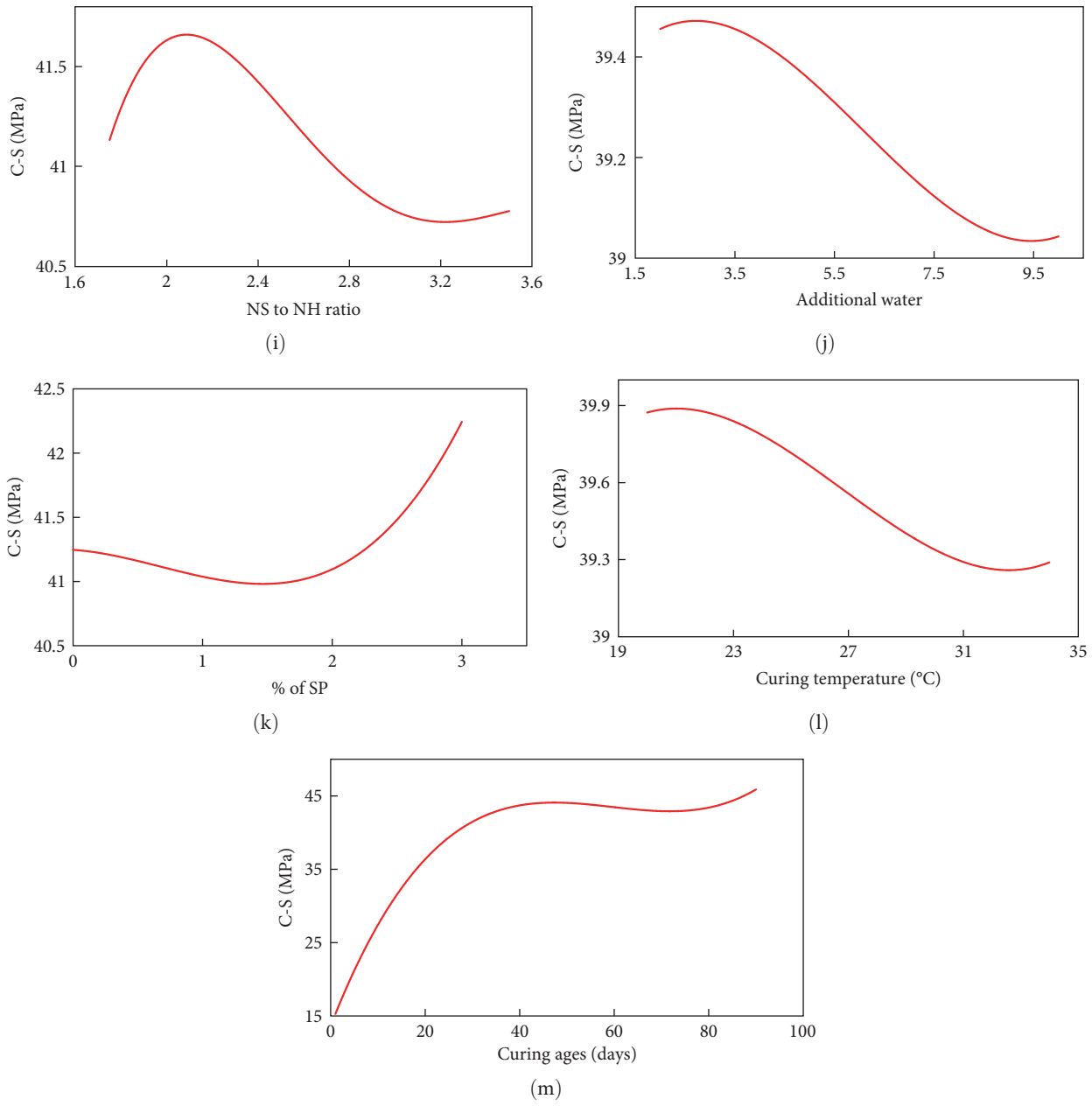

FIGURE 17: Parametric analysis of compressive strength (C-S) with input variables using artificial neural network (ANN) model (a–m). FA, fly ash; NH, sodium hydroxide; NS, sodium silicate; SP, superplasticizer.

optimize model parameters more efficiently or better handle specific data types, improving the overall prediction performance. Additionally, expanding the model to incorporate environmental and durability factors would provide further insights into the long-term performance of GPC, making the model more applicable to real-world engineering scenarios.

4. Conclusions

This study developed an ANN–based model to predict the C-S of GPC by covering a wide range of influencing input parameters. Four regression techniques were employed alongside the ANN model to comprehensively understand the proposed AI approach. This research included the chemical composition of binder materials, excluding the binder type, to generalize and widen the model's applicability, which differed from the prior studies.

The following key findings can be drawn from the study:

a. The ANN–based C-S prediction model shows superior accuracy compared to the model derived from regression analysis. Furthermore, the ANN model demonstrates robust effectiveness across diverse data characteristics, regardless of the material types or

7074, 2024, 1, Downloaded from https://onlinelibrary.wiley.com/doi/10.1155/adce/8534390 by Bangladesh Hinari NPL, Wiley Online Library on [25/01/2025]. See the Terms and Conditions (https://onlinelibrary.wiley.com/terms-and-conditions) on Wiley Online Library for rules of use; OA articles are governed by the applicable Creative Commons License

variables considered as input [84, 86]. In addition, applying the *k*-fold cross-validation approach confirms the satisfactory performance of the ANN model.

b. The ANN model surpasses alternative approaches in prediction effectiveness, as evidenced by the higher R^2 values and lower error rates (RMSE, MAE, and MSE). This superiority is consistently validated by analyzing two additional datasets, further highlighting the enhanced performance of the proposed models compared to existing methods. Parametric analysis further explores that the ANN model can sufficiently incorporate the effects of all influencing input variables used in predicting C-S of GPC.

c. This ANN model dealt with the principal chemical oxides of geopolymer binder to enhance its generalizability, facilitating broader application by avoiding constraints to a specific binder type. Prior studies predominantly centered on the development of AI–based models focused on geopolymer precursors, thus, limiting the data's availability and applicability and confining their relevance to specific binder types.

4.1. Limitations and Future Work. This research intended to include a wide range of parameters influencing GPC strength characteristics; nevertheless, it has limits due to the absence of certain aspects that could affect the C-S of GPC. As this study relies solely on a dataset derived from literature, the lack of real-life experimental data limited the ability to validate the model's predictions. The fresh properties, environmental, and durability parameters that could alter the properties of GPC were not considered. Although the ANN model was compared with traditional regression models, no benchmark against other machine learning techniques was set, such as ensemble methods or deep learning architectures, which could offer further insights into the predictive capabilities.

In addition, while the ANN model showed strong predictive performance, future research could explore other machine learning models such as ensemble methods (e.g., random forest (RF) and gradient boosting machines) or deep learning architectures (e.g., convolutional neural networks and recurrent neural networks). The current model does not account for long-term environmental factors like freeze–thaw cycles, chloride penetration, or carbonation. Including long-term environmental factors in future models would enhance their applicability to real-world durability predictions. Moreover, hybrid models that integrate environmental and mechanical properties could provide a more comprehensive assessment of GPC performance under varied conditions. These models may provide improved accuracy or interpretability in predicting C-S, especially in the context of larger and more complex datasets.

Nomenclature

GPC: geopolymer concrete
C-S: compressive strength
SCMs: supplementary cementitious materials
ANN: artificial neural network
AI: artificial intelligence
SP: superplasticizer
NS: sodium silicate
RMSE: root mean square error
MSE: mean square error
MAE: mean absolute error
R^2: *R*-squared.

Data Availability Statement

The dataset used for all the experiments will be made publicly available upon publication at: https://github.com/AL-MamunProvath17/Strength-Prediction-of-Geopolymer-Concrete-

Ethics Statement

All authors of this manuscript affirm that ethical approval and consent to participate have been secured in compliance with the journal's policies.

Consent

The authors have nothing to report.

Conflicts of Interest

The authors declare no conflicts of interest.

Author Contributions

Md Merajul Islam: conceptualization, data acquisition, methodology, investigation, formal analysis, visualization, writing–original draft. Md Al-Mamun Provath: formal analysis, investigation, resources, modeling, validation, and writing. G. M. Sadiqul Islam: conceptualization, funding acquisition, project administration, supervision, reviewing, and editing. Md Tariqul Islam: investigation, writing–draft. All authors contributed equally and agreed that the manuscript would be published in the International Journal of Concrete Structures and Materials after acceptance.

Funding

The authors received financial support (Project number 37.01.0000.073.06.037.22.421) from the University Grants Commission (UGC) of Bangladesh for the research.

Acknowledgments

The authors sincerely thank the University Grants Commission (UGC) of Bangladesh for funding this project under Project number 37.01.0000.073.06.037.22.421. Appreciation is extended to the Department of Civil Engineering, Chittagong University of Engineering and Technology (CUET), for providing access to research facilities, resources, and a conducive environment that facilitated the smooth progress of this study.

7074, 2024, 1, Downloaded from https://onlinelibrary.wiley.com/doi/10.1155/adce/8534390 by Bangladesh Hinari NPL, Wiley Online Library on [25/01/2025]. See the Terms and Conditions (https://onlinelibrary.wiley.com/terms-and-conditions) on Wiley Online Library for rules of use; OA articles are governed by the applicable Creative Commons License

References

[1] T. R. Naik, "Sustainability of Concrete Construction," *Practice Periodical on Structural Design and Construction* 13-2, no. 2 (2008): 98–103.

[2] C.-K. Ma, A. Z. Awang, and W. Omar, "Structural and Material Performance of Geopolymer Concrete: A Review," *Construction and Building Materials* 186 (2018): 90–102.

[3] B. Singh, G. Ishwarya, M. Gupta, and S. K. Bhattacharyya, "Geopolymer Concrete: A Review of Some Recent Developments," *Construction and Building Materials* 85 (2015): 78–90.

[4] S. Massari and M. Ruberti, "Rare Earth Elements as Critical Raw Materials: Focus on International Markets and Future Strategies," *Resources Policy* 38, no. 1 (2013): 36–43.

[5] S. A. Northey, G. M. Mudd, and T. T. Werner, "Unresolved Complexity in Assessments of Mineral Resource Depletion and Availability," *Natural Resources Research* 27, no. 2 (2018): 241–255.

[6] M. Safiuddin, M. Z. Jumaat, M. A. Salam, M. S. Islam, and R. Hashim, "Utilization of Solid Wastes in Construction Materials," *International Journal of Physical Sciences* 5, no. 13 (2010): 1952–1963.

[7] F. Maghool, A. Arulrajah, Y.-J. Du, S. Horpibulsuk, and A. Chinkulkijniwat, "Environmental Impacts of Utilizing Waste Steel Slag Aggregates as Recycled Road Construction Materials," *Clean Technologies and Environmental Policy* 19, no. 4 (2017): 949–958.

[8] I. Marie and H. Quiasrawi, "Closed-Loop Recycling of Recycled Concrete Aggregates," *Journal of Cleaner Production* 37 (2012): 243–248.

[9] A. Y. Al-Ali, "Assessment of Recycled Aggregate Structural Suitability for Road Construction," 2001, [Online]. Available: https://scholarworks.uaeu.ac.ae/all_thesesTheses.383.https://scholarworks.uaeu.ac.ae/all_theses/383.

[10] A. D. Buck, "Recycled Concrete as a Source of Aggregate," *ACI Journal Proceedings* 74, no. 5 (1977): 212–219.

[11] M. Khan and M. Ali, "Use of Glass and Nylon Fibers in Concrete for Controlling Early Age Micro Cracking in Bridge Decks," *Construction and Building Materials* 125 (2016): 800–808.

[12] J. Xiao, J. Li, and C. Zhang, "Mechanical Properties of Recycled Aggregate Concrete Under Uniaxial Loading," *Cement and Concrete Research* 35, no. 6 (2005): 1187–1194.

[13] E. Vázquez, *Progress of Recycling in the Built Environment* (Springer, 2013).

[14] P. Duxson, A. Fernández-Jiménez, J. L. Provis, G. C. Lukey, A. Palomo, and J. S. J. van Deventer, "Geopolymer Technology: The Current State of the Art," *Journal of Materials Science* 42, no. 9 (2007): 2917–2933.

[15] A. Mehta, R. Siddique, T. Ozbakkaloglu, F. U. A. Shaikh, and R. Belarbi, "Fly Ash and Ground Granulated Blast Furnace Slag-Based Alkali-Activated Concrete: Mechanical, Transport and Microstructural Properties," *Construction and Building Materials* 257 (2020): 119548.

[16] L. Guo, Y. Wu, F. Xu, et al., "Sulfate Resistance of Hybrid Fiber Reinforced Metakaolin Geopolymer Composites," *Composites Part B: Engineering* 183 (2020): 107689.

[17] M. Albitar, M. S. M. Ali, P. Visintin, and M. Drechsler, "Durability Evaluation of Geopolymer and Conventional Concretes," *Construction and Building Materials* 136 (2017): 374–385.

[18] A. Karthik, K. Sudalaimani, and C. T. Vijayakumar, "Durability Study on Coal Fly Ash-Blast Furnace Slag Geopolymer Concretes With Bio-Additives," *Ceramics International* 43, no. 15 (2017): 11935–11943.

[19] D. Adak, M. Sarkar, and S. Mandal, "Effect of Nano-Silica on Strength and Durability of Fly Ash Based Geopolymer Mortar," *Construction and Building Materials* 70 (2014): 453–459.

[20] H. U. Ahmed, A. A. Mohammed, and A. S. Mohammed, "Effectiveness of Silicon Dioxide Nanoparticles (Nano SiO2) on the Internal Structures, Electrical Conductivity, and Elevated Temperature Behaviors of Geopolymer Concrete Composites," *Journal of Inorganic and Organometallic Polymers and Materials* 33, no. 12 (2023): 3894–3914.

[21] B. C. McLellan, R. P. Williams, J. Lay, A. van Riessen, and G. D. Corder, "Costs and Carbon Emissions for Geopolymer Pastes in Comparison to Ordinary Portland Cement," *Journal of Cleaner Production* 19, no. 9-10 (2011): 1080–1090.

[22] V. D. Cao, S. Pilehvar, C. Salas-Bringas, et al., "Microencapsulated Phase Change Materials for Enhancing the Thermal Performance of Portland Cement Concrete and Geopolymer Concrete for Passive Building Applications," *Energy Conversion and Management* 133 (2017): 56–66.

[23] W. Ahmad, S. H. Farooq, M. Usman, et al., "Effect of Coconut Fiber Length and Content on Properties of High Strength Concrete," *Materials* 13, no. 5 (2020): 1075.

[24] K. Somna, C. Jaturapitakkul, P. Kajitvichyanukul, and P. Chindaprasirt, "NaOH-Activated Ground Fly Ash Geopolymer Cured at Ambient Temperature," *Fuel* 90, no. 6 (2011): 2118–2124.

[25] S. Y. Oderji, B. Chen, M. R. Ahmad, and S. F. A. Shah, "Fresh and Hardened Properties of One-Part Fly Ash-Based Geopolymer Binders Cured at Room Temperature: Effect of Slag and Alkali Activators," *Journal of Cleaner Production* 225 (2019): 1–10.

[26] P. Chindaprasirt, P. De Silva, K. Sagoe-Crentsil, and S. Hanjitsuwan, "Effect of SiO2 and Al2O 3 on the Setting and Hardening of High Calcium Fly Ash-Based Geopolymer Systems," *Journal of Materials Science* 47, no. 12 (2012): 4876–4883.

[27] S. Prasanphan, A. Wannagon, T. Kobayashi, and S. Jiemsirilers, "Reaction Mechanisms of Calcined Kaolin Processing Waste-Based Geopolymers in the Presence of Low Alkali Activator Solution," *Construction and Building Materials* 221 (2019): 409–420.

[28] A. A. Mohammed, H. U. Ahmed, and A. Mosavi, "Survey of Mechanical Properties of Geopolymer Concrete: A Comprehensive Review and Data Analysis," *Materials* 14, no. 16 (2021): 4690.

[29] A. Hassan, M. Arif, and M. Shariq, "Effect of Curing Condition on the Mechanical Properties of Fly Ash-Based Geopolymer Concrete," *SN Applied Sciences* 1 (2019): 1694.

[30] A. A. Aliabdo, A. E. M. Abd Elmoaty, and H. A. Salem, "Effect of Water Addition, Plasticizer and Alkaline Solution Constitution on Fly Ash Based Geopolymer Concrete Performance," *Construction and Building Materials* 121 (2016): 694–703.

[31] T. Phoo-ngernkham, C. Phiangphimai, N. Damrongwiriyanupap, S. Hanjitsuwan, J. Thumrongvut, and P. Chindaprasirt, "A Mix Design Procedure for Alkali-Activated High-Calcium Fly Ash Concrete Cured at Ambient Temperature," *Advances in Materials Science and Engineering* 2018, no. 1 (2018): 2460403.

[32] N. Nikoloutsopoulos, A. Sotiropoulou, G. Kakali, and S. Tsivilis, "Physical and Mechanical Properties of Fly Ash Based Geopolymer Concrete Compared to Conventional Concrete," *Buildings* 11, no. 5 (2021): 178.

7074, 2024, 1, Downloaded from https://onlinelibrary.wiley.com/doi/10.1155/adce/8534390 by Bangladesh Hinari NPL, Wiley Online Library on [25/01/2025]. See the Terms and Conditions (https://onlinelibrary.wiley.com/terms-and-conditions) on Wiley Online Library for rules of use; OA articles are governed by the applicable Creative Commons License

[33] G. Jiang, J. Keller, P. L. Bond, and Z. Yuan, "Predicting Concrete Corrosion of Sewers Using Artificial Neural Network," *Water Research* 92 (2016): 52–60.

[34] A. A. Elshafey, N. Dawood, H. Marzouk, and M. Haddara, "Crack Width in Concrete Using Artificial Neural Networks," *Engineering Structures* 52 (2013): 676–686.

[35] F. Khademi, S. M. Jamal, N. Deshpande, and S. Londhe, "Predicting Strength of Recycled Aggregate Concrete Using Artificial Neural Network, Adaptive Neuro-Fuzzy Inference System and Multiple Linear Regression," *International Journal of Sustainable Built Environment* 5, no. 2 (2016): 355–369.

[36] D.-K. Bui, T. Nguyen, J.-S. Chou, H. Nguyen-Xuan, and T. D. Ngo, "A Modified Firefly Algorithm-Artificial Neural Network Expert System for Predicting Compressive and Tensile Strength of High-Performance Concrete," *Construction and Building Materials* 180 (2018): 320–333.

[37] M. Ahmadi, H. Naderpour, and A. Kheyroddin, "Utilization of Artificial Neural Networks to Prediction of the Capacity of CCFT Short Columns Subject to Short Term Axial Load," *Archives of Civil and Mechanical Engineering* 14, no. 3 (2014): 510–517.

[38] H. M. Tanarslan, M. Secer, and A. Kumanlioglu, "An Approach for Estimating the Capacity of RC Beams Strengthened in Shear With FRP Reinforcements Using Artificial Neural Networks," *Construction and Building Materials* 30 (2012): 556–568.

[39] R. Perera, M. Barchín, A. Arteaga, and A. D. Diego, "Prediction of the Ultimate Strength of Reinforced Concrete Beams FRP-Strengthened in Shear Using Neural Networks," *Composites Part B: Engineering* 41, no. 4 (2010): 287–298.

[40] H. Naderpour, O. Poursaeidi, and M. Ahmadi, "Shear Resistance Prediction of Concrete Beams Reinforced by FRP Bars Using Artificial Neural Networks," *Measurement* 126 (2018): 299–308.

[41] C. T. Leondes, "Introduction to Software Engineering / Print Version Table of Contents," 2017, Accessed: Jun. 06, 2023. [Online]. Available: https://www.routledge.com/Intelligent-Systems-Technology-and-Applications-Six-Volume-Set/Leondes/p/book/9780849311215.

[42] R. A. Mozumder and A. I. Laskar, "Prediction of Unconfined Compressive Strength of Geopolymer Stabilized Clayey Soil Using Artificial Neural Network," *Computers and Geotechnics* 69 (2015): 291–300.

[43] A. Nazari, "Artificial Neural Networks Application to Predict the Compressive Damage of Lightweight Geopolymer," *Neural Computing and Applications* 23, no. 2 (2013): 507–518.

[44] İ. B. Topçu and M. Sarıdemir, "Prediction of Compressive Strength of Concrete Containing Fly Ash Using Artificial Neural Networks and Fuzzy Logic," *Computational Materials Science* 41, no. 3 (2008): 305–311.

[45] B. K. R. Prasad, H. Eskandari, and B. V. V. Reddy, "Prediction of Compressive Strength of SCC and HPC With High Volume Fly Ash Using ANN," *Construction and Building Materials* 23, no. 1 (2009): 117–128.

[46] F. J. de Cos Juez, F. S. Lasheras, N. Roqueñí, and J. Osborn, "An ANN-Based Smart Tomographic Reconstructor in a Dynamic Environment," *Sensors* 12, no. 7 (2012): 8895–8911.

[47] A. Nazari and F. P. Torgal, "Predicting Compressive Strength of Different Geopolymers by Artificial Neural Networks," *Ceramics International* 39, no. 3 (2013): 2247–2257.

[48] M. M. Yadollahi, A. Benli, and R. Demirboğa, "Prediction of Compressive Strength of Geopolymer Composites Using an Artificial Neural Network," *Materials Research Innovations* 19, no. 6 (2015): 453–458.

[49] S. Nagajothi and S. Elavenil, "Influence of Aluminosilicate for the Prediction of Mechanical Properties of Geopolymer Concrete—Artificial Neural Network," *Silicon* 12, no. 5 (2020): 1011–1021.

[50] "(PDF) Modeling of Compressive Strength of Metakaolin Based Geopolymers by the use of Artificial Neural Network," 2023, (accessed Jun. 07 https://www.researchgate.net/publication/279900967_Modeling_of_compressive_strength_of_Metakaolin_based_geopolymers_by_the_use_of_artificial_neural_network.

[51] D. Bondar, "Use of a Neural Network to Predict Strength and Optimum Compositions of Natural Alumina-Silica-Based Geopolymers," *Journal of Materials in Civil Engineering* 26, no. 3 (2014): 499–503.

[52] A. Nazari, S. Riahi, G. Khalaj, H. Bohlooli, and M. M. Kaykha, "Prediction of Compressive Strength of Geopolymers With Seeded Fly Ash and Rice Husk-Bark Ash by Gene Expression Programming," *International Journal of Damage Mechanics* 21, no. 8 (2012): 1202–1226.

[53] H. U. Ahmed, A. S. Mohammed, and A. A. Mohammed, "Proposing Several Model Techniques including ANN and M5P-Tree to Predict the Compressive Strength of Geopolymer Concretes Incorporated With Nano-Silica," *Environmental Science and Pollution Research* 29, no. 47 (2022): 71232–71256.

[54] D. B. Vidivelli, "Prediction of Compressive Strength of High Performance Concrete Containing Industrial by Products Using Artificial Neural Networks," (2016).

[55] P. Chopra, R. K. Sharma, and M. Kumar, "Prediction of Compressive Strength of Concrete Using Artificial Neural Network and Genetic Programming," *Advances in Materials Science and Engineering* 2016 (2016): 7648467.

[56] H. Song, A. Ahmad, K. A. Ostrowski, and M. Dudek, "Analyzing the Compressive Strength of Ceramic Waste-Based Concrete Using Experiment and Artificial Neural Network (Ann) Approach," *Materials* 14, no. 16 (2021): 4518.

[57] M. Sarıdemir, "Predicting the Compressive Strength of Mortars Containing Metakaolin by Artificial Neural Networks and Fuzzy Logic," *Advances in Engineering Software* 40, no. 9 (2009): 920–927.

[58] S. Gupta, "Using Artificial Neural Network to Predict the Compressive Strength of Concrete Containing Nano-Silica," *Civil Engineering and Architecture* 1, no. 3 (2013): 96–102.

[59] J. Huang, Y. Sun, and J. Zhang, "Reduction of Computational Error by Optimizing SVR Kernel Coefficients to Simulate Concrete Compressive Strength Through the Use of a Human Learning Optimization Algorithm," *Engineering With Computers* 38, no. 4 (2022): 3151–3168.

[60] A. Ahmad, F. Farooq, K. A. Ostrowski, K. Śliwa-Wieczorek, and S. Czarnecki, "Application of Novel Machine Learning Techniques for Predicting the Surface Chloride Concentration in Concrete Containing Waste Material," *Materials* 14, no. 9 (2021): 2297.

[61] M. Azimi-Pour, H. Eskandari-Naddaf, and A. Pakzad, "Linear and Non-Linear SVM Prediction for Fresh Properties and Compressive Strength of High Volume Fly Ash Self-Compacting Concrete," *Construction and Building Materials* 230 (2020): 117021.

[62] A. A. Shahmansouri, H. A. Bengar, and E. Jahani, "Predicting Compressive Strength and Electrical Resistivity of Eco-Friendly Concrete Containing Natural Zeolite via GEP Algorithm," *Construction and Building Materials* 229 (2019): 116883.

7074, 2024, 1, Downloaded from https://onlinelibrary.wiley.com/doi/10.1155/adce/8534390 by Bangladesh Hinari NPL, Wiley Online Library on [25/01/2025]. See the Terms and Conditions (https://onlinelibrary.wiley.com/terms-and-conditions) on Wiley Online Library for rules of use; OA articles are governed by the applicable Creative Commons License

[63] P. G. Asteris and K. G. Kolovos, "Self-Compacting Concrete Strength Prediction Using Surrogate Models," *Neural Computing and Applications* 31, no. S1 (2019): 409–424.
[64] J. Zhang, G. Ma, Y. Huang, J. sun, F. Aslani, and B. Nener, "Modelling Uniaxial Compressive Strength of Lightweight Self-Compacting Concrete Using Random Forest Regression," *Construction and Building Materials* 210 (2019): 713–719.
[65] O. B. Douma, B. Boukhatem, M. Ghrici, and A. Tagnit-Hamou, "Prediction of Properties of Self-Compacting Concrete Containing Fly Ash Using Artificial Neural Network," *Neural Computing and Applications* 28, no. S1 (2017): 707–718.
[66] M. Abu Yaman, M. Abd Elaty, and M. Taman, "Predicting the Ingredients of Self Compacting Concrete Using Artificial Neural Network," *Alexandria Engineering Journal* 56, no. 4 (2017): 523–532.
[67] A. Ahmad, F. Farooq, P. Niewiadomski, et al., "Prediction of Compressive Strength of Fly Ash Based Concrete Using Individual and Ensemble Algorithm," *Materials* 14, no. 4 (2021): 794.
[68] C. Bilim, C. D. Atiş, H. Tanyildizi, and O. Karahan, "Predicting the Compressive Strength of Ground Granulated Blast Furnace Slag Concrete Using Artificial Neural Network," *Advances in Engineering Software* 40, no. 5 (2009): 334–340.
[69] F. Özcan, C. D. Atiş, O. Karahan, E. Uncuoğlu, and H. Tanyildizi, "Comparison of Artificial Neural Network and Fuzzy Logic Models for Prediction of Long-Term Compressive Strength of Silica Fume Concrete," *Advances in Engineering Software* 40, no. 9 (2009): 856–863.
[70] M. Sarıdemir, "Prediction of Compressive Strength of Concretes Containing Metakaolin and Silica Fume by Artificial Neural Networks," *Advances in Engineering Software* 40, no. 5 (2009): 350–355.
[71] Y. Ling, K. Wang, X. Wang, and W. Li, "Prediction of Engineering Properties of Fly Ash-Based Geopolymer Using Artificial Neural Networks," *Neural Computing and Applications* 33, no. 1 (2021): 85–105.
[72] D. Van Dao, H. B. Ly, S. H. Trinh, T. T. Le, and B. T. Pham, "Artificial Intelligence Approaches for Prediction of Compressive Strength of Geopolymer Concrete," *Materials* 12, no. 6 (2019): 983.
[73] Y. Lin, C. P. Lai, and T. Yen, "Prediction of Ultrasonic Pulse Velocity (UPV) in Concrete," *ACI Materials Journal* 100, no. 1 (2003): 21–28.
[74] G. Trtnik, F. Kavčič, and G. Turk, "Prediction of Concrete Strength Using Ultrasonic Pulse Velocity and Artificial Neural Networks," *Ultrasonics* 49, no. 1 (2009): 53–60.
[75] S.-T. Yi, E.-I. Yang, and J.-C. Choi, "Effect of Specimen Sizes, Specimen Shapes, and Placement Directions on Compressive Strength of Concrete," *Nuclear Engineering and Design* 236, no. 2 (2006): 115–127.
[76] C. Jithendra and S. Elavenil, "Influences of Parameters on Slump Flow and Compressive Strength Properties of Aluminosilicate Based Flowable Geopolymer Concrete Using Taguchi Method," *Silicon* 12, no. 3 (2020): 595–602.
[77] P. G. Asteris, M. Karoglou, A. D. Skentou, et al., "Predicting Uniaxial Compressive Strength of Rocks Using ANN Models: Incorporating Porosity, Compressional Wave Velocity, and Schmidt Hammer Data," *Ultrasonics* 141 (2024): 107347.
[78] I.-C. Yeh, "Modeling of Strength of High-Performance Concrete Using Artificial Neural Networks," *Cement and Concrete Research* 28, no. 12 (1998): 1797–1808.
[79] S. K. Das, J. Mishra, S. K. Singh, et al., "Characterization and Utilization of Rice Husk Ash (RHA) in Fly Ash—Blast Furnace Slag Based Geopolymer Concrete for Sustainable Future," *Materials Today: Proceedings* 33 (2020): 5162–5167.
[80] P. Nath and P. K. Sarker, "Effect of GGBFS on Setting, Workability and Early Strength Properties of Fly Ash Geopolymer Concrete Cured in Ambient Condition," *Construction and Building Materials* 66 (2014): 163–171.
[81] S. R. K. Reddy and S. B. Murugan, "Experimental and Microstructural Assessment of Ternary Blended Geopolymer Concrete With Different Na2SiO3-to-NaOH Volume Ratios," *Innovative Infrastructure Solutions* 5, no. 1 (2020): 1–14.
[82] A. Niş, "Compressive Strength Variation of Alkali Activated Fly Ash/Slag Concrete With Different NaOH Concentrations and Sodium Silicate to Sodium Hydroxide Ratios," *Journal of Sustainable Construction Materials and Technologies* 4, no. 2 (2019): 351–360.
[83] Y. Jung and Y. Kim, "A Study on the Compressive Strength Properties of the Ternary Blended Non-Cement Concrete Using Ternary Diagram," *Journal of the Korea Institute for Structural Maintenance and Inspection* 24, no. 2 (2020): 41–49.
[84] M. A. Khan, A. Zafar, F. Farooq, et al., "Geopolymer Concrete Compressive Strength via Artificial Neural Network, Adaptive Neuro Fuzzy Interface System, and Gene Expression Programming With K-Fold Cross Validation," *Frontiers in Materials* 8 (2021): 1–19.
[85] M. A. Hossain, G. M. S. Islam, and A. Mallick, "Compressive Strength Prediction for Industrial Waste-Based SCC Using Artificial Neural Network," *Journal of the Civil Engineering Forum* (2022): 11–26.
[86] M. A. Khan, S. A. Memon, F. Farooq, M. F. Javed, F. Aslam, and R. Alyousef, "Compressive Strength of Fly-Ash-Based Geopolymer Concrete by Gene Expression Programming and Random Forest," *Advances in Civil Engineering* 2021 (2021): 6618407.

7074, 2024, 1, Downloaded from https://onlinelibrary.wiley.com/doi/10.1155/adce/8534390 by Bangladesh Hinari NPL, Wiley Online Library on [25/01/2025]. See the Terms and Conditions (https://onlinelibrary.wiley.com/terms-and-conditions) on Wiley Online Library for rules of use; OA articles are governed by the applicable Creative Commons License